

We thank the reviewers for their time and effort reviewing this manuscript. All reviewer comments are reproduced below in ***bold, italicized font***. Our responses are shown in regular font. Changes to the text are indicated as underlined text for insertions or are ~~crossed-out~~ for deletions. Line numbers given below are for the revised version with all markups shown. We numbered the reviewer comments for easier cross-referencing.

Anonymous Referee #1

Received and published: 21 May 2018

Taha et al., report an approach to quantifying peroxyacetyl nitrates (PANs and PANs) by combining the techniques of differential thermal dissociation (TD), peroxy radical chemical amplification (PERCA) and cavity ring down spectrum for NO₂ detection (CRDS), named TD-PERCA-CRDS. The instrument has single channel (on-off mode), dual channel (background NO₂, background + amplified NO₂) and four channel detection modes (differential temperature measurement). The chemical amplification module is optimized by injecting 0.6 ppm NO and 1.6% C₂H₆, the chain length (CL) is range from 20 to 70. They found that the measurement was suffered with the ambient O₃ interferences by thermal dissociating O₃ to O above 150 oC and the following reaction with ethane; the differential temperature TD-PERCA-CRDS at 60110 oC was also unfeasible in ambient due to the unknown interferences in ambient air.

Compared with TD-CRDS /LIF/CAPS, this technique still can't be well performed in field measurement, while the adding of PERCA provide a way to improve the detecting capacity of PANs and PANs to several pptv level. Overall the manuscript is well written and would be of interest and contribute to the community, I recommend this paper to be published on AMT subject to these comments below.

We thank the reviewer for these kind comments.

Major comments:

1. This instrument can calibrate the CL for several PANs or PPN produced in the lab at certain temperature and RH, but the CL is highly varied for different kinds of peroxyacetyl nitrates in ambient conditions, which also prevent the application of field measurement.

We agree that the variability of the chain lengths is a challenge and acknowledge that field measurements will require further work before they can become a reality (lines 492): "... the TD-PERCA-CRDS method has several drawbacks, some of which still need to be overcome to make ambient measurements a reality."

However, these are unsurmountable. Variable chain lengths also occur in regular PERCA instruments, and this has not prevented measurement of OH and ΣRO₂ with those instruments. Since the main chain carriers are OH and HO₂, and the chain lengths are large, the variability is not because of the nature of the radical precursor, but rather functions of temperature, humidity, and reagent gas concentrations. As we stated on line 507, frequent calibrations will be a necessity for this reason.

We have not amended the manuscript in response to this comment.

2. Is it possible to carry out the simultaneous measurement of CIMS with the four channel detection measurement in ambient condition to look insight of the unknown species? CIMS measurement might provide some useful information about the unknown interference.

This is an interesting suggestion. With CIMS operated with iodide reagent ion, it is certainly possible to quantify HNO₄, PAN, PPN, etc., and much could be learned from a side-by-side comparison. It could, for example, give insight into the magnitude and time-of-day dependence of the interference.

We have added to the following on line 532:

"Furthermore, such measurements should be complemented by parallel measurements of PNA, PAN and PPN by CIMS."

Specific comments:

1. Line 105, if the majority of the experiments conducted by single-channel TDPERCA-CRDS, the schematic figure of the single channel is worth to be shown in Figure 1.

This schematic is shown in the Electronic Supplementary Material of (Taha et al., 2018), which is subject to copyright. We have therefore chosen not to reproduce it here, but altered to the text on line 105 as follows:

"The majority of the experiments described in this manuscript were conducted using a single-channel TD-PERCA inlet that is described and depicted as Figure S1 of the Electronic Supplementary Material ~~ohas been described elsewhere~~ (Taha et al., 2018)."

2. Line 45 and line 457: "10s to a few 100s" change to "tens to a few hundreds of".

We have changed the manuscript as requested by the reviewer.

3. Line 228, it is not necessary to set the single sentence to a paragraph.

This has been corrected.

4. The format of tables (1-6) does not conform to the academic norm.

We believe the reviewer is referring to the following instructions (taken from the Manuscript preparation guidelines for authors) on the AMT web site:

"Horizontal lines should normally only appear above and below the table, and as a separator between the head and the main body of the table. Vertical lines must be avoided."

We have amended the table borders as per the above instructions.

5. Section 3.5.2, suggest the authors unify all the units to be pptv.

We have changed the manuscript as suggested by the reviewer.

6. Line 893 the legend in Figure 7. (A): "Legend Sample time series of PNA observed by TD-PERCA-CRDS in the reference, NO₂ channel (shown in green) and PERCA channel (grey)." is not consist with the description in line 274, please correct it.

We apologize - the colors were reversed in Figure 7A. NO₂ is now shown in green, and the heated channel in ash (aka grey) colour, consistent with the main text (lines 275-280) and the caption of Figure 7A.

7. Is figure 8(A) only show part of the data presented in figure 7(A), as we can see the maximum NO₂ in figure 7(A) was about 20 ppbv while in figure 8(A) the maximum was only 16 ppbv. The authors should clarify it.

Figure 8A was set to <0.6 ppbv on the x-axis and <16 ppbv on the y axis, as this was the linear dynamic range. We updated the figure to show the entire concentration range and also moved the result of the linear fits (slope, intercept and r²) to the figure caption for clarity.

8. Figure 10 shows the CL dependence on the radical concentration (PAN, PPN and PNA), the PNA seems decreasing with the increasing of PNA concentration, and in line 320-335, no text gave the description or explanation about PNA dependence, I suggest adding some words to describe the CL dependence on the PNA concentration.

We agree with the reviewer that the PNA data in Figure 10 at first glance look as if they decrease with concentration. However, looks are deceiving in this case since this trend falls within the scatter of the individual measurements, and Figure 8A clearly shows the absence of a concentration dependence. The main chain carriers are identical (HO₂ and OH) for PAN and PNA, such that one would expect the dynamic range for PNA to be the same as that for PAN or PPN, so PNA does not need to be discussed separately.

We modified a sentence on line 324 to make this clearer:

"It is well known in the PERCA community that the chain lengths decrease at high radical concentrations due to radical-radical reactions. Figures 8A and 8B demonstrate that the response of TD-PERCA-CRDS is linear for both PNA and PAN/PPN at low, atmospherically relevant mixing ratios (i.e., below ~600 pptv). The linear dynamic range is similar for PNA and PAN and PPN since the radical chain carriers are the same for both."

9. I suggest the authors summarizing the existed TD techniques that applied in the field measurement of peroxyacetyl nitrate or peroxyacetyl nitrates, which offers convenience to the readers and contributes to the community.

We have added a Table summarizing TD techniques on line 783 as requested by the reviewer.

Table 2. Selected thermal dissociation methods for quantification of daytime NO_y species.

<u>Species quantified</u>	<u>NO₂ detection method</u>	<u>Group</u>	<u>Reference</u>
<u>NO₂, ΣPAN, ΣAN, HNO₃</u>	<u>LIF</u>	<u>Berkeley</u>	<u>(Day et al., 2002)</u>
<u>ΣPN</u>	<u>LIF</u>	<u>Berkeley</u>	<u>(Murphy et al., 2004)</u>
<u>HONO</u>	<u>CL</u>	<u>Berkeley</u>	<u>(Perez et al., 2007)</u>
<u>NO₂, ΣPAN, ΣAN</u>	<u>CRDS</u>	<u>Calgary</u>	<u>(Paul et al., 2009)</u>
<u>Aerosol nitrates</u>	<u>LIF</u>	<u>Berkeley</u>	<u>(Rollins et al., 2010)</u>
<u>ClNO₂</u>	<u>CRDS</u>	<u>Calgary</u>	<u>(Thaler et al., 2011)</u>
<u>NO₂, ΣPAN, ΣAN, HNO₃</u>	<u>LIF</u>	<u>L'Aquila</u>	<u>(Di Carlo et al., 2013)</u>
<u>NO, NO₂, HONO, NO_y, ammonium nitrate</u>	<u>CRDS</u>	<u>NOAA</u>	<u>(Wild et al., 2014; Womack et al., 2017)</u>
<u>NO₂, ΣPAN, ΣAN</u>	<u>CRDS</u>	<u>Max-Planck-Institut</u>	<u>(Thieser et al., 2016)</u>
<u>NO₂, ΣPAN, ΣAN</u>	<u>CAPS</u>	<u>Osaka</u>	<u>(Sadanaga et al., 2016)</u>
<u>NO₂, RNO₂</u>	<u>CRDS</u>	<u>Hefei</u>	<u>(Chen et al., 2017b)</u>
<u>ΣPN, ΣPAN</u>	<u>PERCA-CRDS</u>	<u>Calgary</u>	<u>this work</u>

Anonymous Referee #2

Received and published: 5 June 2018

This paper describes laboratory characterization of a new method for quantifying peroxyacetic acid (PNA) and peroxyacyl nitrates. Overall the article is well written and describes important results and I recommend publication after the mostly minor issues below are addressed.

We also thank reviewer #2 for this assessment.

Line 79: "The measurement of peroxy radicals by PERCA is prone to interferences", but the text proceeds to discuss that the amplification must be determined by calibrations and that it varies with relative humidities. These are not interferences! Later in the text an actual interference by ozone for TD-PERCA_CRDS is well described But variation of calibration factor with RH is not an interference.

The reviewer is correct, of course. We modified the text on line 79 as follows:

"The measurement of peroxy radicals by PERCA is prone to matrix effects and interferences. For instance, a key operational parameter of any PERCA instrument is the radical chain length or amplification factor (CL), ..."

Same for 89: replace "interference" with "disadvantage" or "property"?

The thermal decomposition of PAN produces radicals and interferes in the measurement of RO_x radicals by PERCA, so we believe that the word "interference" is used correctly in this context.

We modified the text on line 87 to improve its clarity:

"... apply heat. When quantification of ambient RO_x radicals is the goal, this is avoided to prevent TD of ΣPN or ΣPAN (which are more abundant than free RO_x radicals). TD of ΣPN or ΣPAN produces radicals that as these molecules would interfere with the measurement of free RO_x radicals (Mihele and Hastie, 2000). On the other hand, if measurement of ΣPN or ΣPAN is desired (such as in this paper), this interference is turned into a measurement principle. "

Ling 143 – "Teflon" – what kind – PFA? PTFE?

It is FEP. We inserted "fluorinated ethylene propylene (FEP)" prior to Teflon on line 145.

Section 2.3.2 – clarify that the concentration of PNA is determined by the NO₂ mixing ratio, correct? ie, NO₂ is the limiting reagent and HO₂ is in excess.

The mixing ratio of HO₂NO₂ delivered by this source was quantified by TD-CRDS (i.e., the difference in [NO₂] between the heated and room temperature channel.

We added the following sentence on line 194:

"The amount of PNA delivered from this source was quantified by TD-CRDS."

Line 190-191 – O₂ is not readily photolyzed to form O₃ by 254 nm – replace with "...generated by photolysis of O₂ by 185 nm radiation from a low-pressure mercury lamp"?

We used a 254 nm lamp as stated in the text - both the 254 and 185 nm version will photo-dissociate O₂. The 185 nm one generates way too much O₃ for our particular application, however.

We have not amended the manuscript in response to this comment.

Box model simulations (in SI) The SI discusses formation of C₂H₅ONO and C₂H₅O₂NO₂, but what about the temperature dependence of C₂H₅ONO₂? That is, ethyl nitrate, formed by C₂H₅O₂ + NO.

The reviewer is referring to section S1.4, where we discuss molecules whose formation is not included in the MCM. Formation of ethyl nitrate is included in the MCM and did not need to be discussed in this section.

For C₂H₅O₂ + NO → C₂H₅ONO₂, the MCM rate expression is $2.25 \times 10^{-14} \times e^{(380/T)}$, i.e., the reaction has a negative activation energy and slows down at higher temperatures. The branching ratio (relative to C₂H₅O₂ + NO → C₂H₅O + NO₂) is 0.9%, which implies that this reaction is an important radical sink especially at higher chain lengths (in the simulations, anyhow).

However, a general problem with using the MCM to simulate TD-PERCA chamber kinetics is that rate constant expressions in the MCM are for atmospheric temperature regimes, i.e., < 300 K. We acknowledged this limitation in section S1.0 "An additional limitation is that the MCM has only been validated at ambient temperature and below, and the rate constants are more uncertain at elevated temperatures."

We agree with the reviewer that the temperature dependence of ethyl nitrate formation may perhaps be worth another look at. However, given that this would be speculation only, we have chosen not to wade into this discussion and have not altered the manuscript in response to this comment.

Section 3.2 and figure 5. This is overall very good demonstration of the technique. It is a bit confusing that, apparently, both the inlet heater and PERCA chamber can be heated separately. This should be more explicitly pointed out in the earlier experimental sections.

The reviewer is correct that we can apply heat to two separate inlet sections.

We added the following on line 117:

"The remaining two channels were equipped with heated quartz tubes to monitor NO₂ + ΣPAN and NO₂ + ΣPAN + total alkyl nitrates (ΣAN) (Paul et al., 2009)."

and modified the text in section 3.2 (lines 234-241) as follows:

"A time series demonstrating amplification of PAN and PPN in the TD-PERCA-CRDS ~~operated with its inlet at 250 °C~~ is shown in Figure 5. In this experiment, PAN and PPN were delivered via the preparatory-scale GC (Figure 2), and the single-channel setup (section 2.1.1) was used.

PAN and PPN eluted from the GC column after 3 min and 6 min, respectively. The compounds eluted as plateaus because of the relatively long (~30 s) injection time. In Figure 5A, PAN and PPN are observed only by the heated (NO₂+ ΣPAN) TD-CRDS channel. This channel was operated with its quartz inlet at 250 °C where they to quantitatively (see Figure 5 of (Paul et al., 2009)) decompose PAN and PPN to NO₂+~~at~~. In this example, mixing ratios of 2.00±0.09 ppbv and 1.86±0.12 ppbv were observed, respectively (errors are 1 σ of 1 s data)."

Ling 281: the text in the parenthesis, though likely true, makes the sentence awkward to read

We agree and have removed the text in the parenthesis.

Section 3.5: interestingly the amplification factor for PNA (yielding HO₂) is less than that for PAN (which forms CH₃CO₃). The following sections address details of the chain length with T, RH, but is there is a conclusion for why the PNA vs. PAN results are so different?

Yes, the amplification factor itself is temperature dependent. An entire section of text (section 3.5.3) is devoted to this. Specifically, line 350-353 state that "It is obvious from Figure 11 that the amplification factor is strongly dependent on temperature: Even though PNA fully dissociates at temperatures > ~90 °C in our inlets (Figure 4), the amplified signal increases by ~60% in the region from 90 °C to 135 °C (Figure 11, insert), corresponding to amplification factors of ~15 and ~22, respectively. This increase is qualitatively consistent (if extrapolated) with the higher amplification factor observed with PAN or PPN at 250 °C."

We have not amended the manuscript in response to this comment.

Line 309: “ : : operated under optimal conditions and : : ” – this assumes that the optimal conditions do not change under varying circumstances. Might it be possible that the optimum NO or ethane concentrations are different at different temperatures or RH values?

It's possible, though we don't believe that the optimum concentrations would change by much. However, since we didn't re-optimize at every RH and temperature, the reviewer has a point that we cannot claim that that TD-CRDS was operated optimally throughout. What we tried to say was that NO and ethane concentrations were constant in these experiments; these mixing ratios are stated in the caption of Figure 9.

We have modified the text on line 312 as follows:

"... the RH dependence was investigated systematically at constant NO and ethane concentrations with TD-PERCA-CRDS operated under optimal conditions and with PAN and PPN at 250 °C inlet temperature. The results are summarized in Figure 9."

Section 3.7.2: The observed interferences are very interesting, and are likely relevant not only to TD-PERCA-CRDS but also to non-amplified thermal dissociation methods, e.g. TD-LIF.

This is conceivable, but unlikely. The ethane-PERCA will amplify any molecule that generates trace levels OH, HO₂, RO₂, RO, or O when heated; in un-amplified TD, concentrations of these radicals are likely too small to have much impact. The only exception is, perhaps, O₃, which generates O, that can react with NO₂ to NO and O₂. Ron Cohen's group is aware of this: In Atmos. Chem. Phys., 14, 12441-12454, 10.5194/acp-14-12441-2014, 2014, Appendix A, Lee et al. discuss the impacts of O₃ pyrolysis in their system.

We have not amended the manuscript in response to this comment.

Section 3.8, discussion of detection limit. Some of the terms here are confusing.

1. Do the authors actually mean precision when they have written LOD? LOD needs to be defined – is it for signal to noise ratio of 2? Or 3? The LOD is quoted as 87 ppt (1 sigma, 1 sec), but this seems much more like a description of the precision, not the LOD (ie, 1 sigma for precision, signal to noise ratio for LOD).

We agree with the reviewer that this section requires a few clarification.

Detection limit is defined by the International Union of Pure and Applied Chemistry (IUPAC) (<https://goldbook.iupac.org/html/L/L03540.html>) as follows: "The limit of detection, expressed as the concentration, c_L, or the quantity, q_L, is derived from the smallest measure, x_L, that can be detected with reasonable certainty for a given analytical procedure. The value of x_L is given by the equation

$$x_L = \bar{x}_{bi} + k s_{bi}$$

where \bar{x}_{bi} is the mean of the blank measures, s_{bi} is the standard deviation of the blank measures, and k is a numerical factor chosen according to the confidence level desired."

In CRDS, \bar{x}_{bi} equals zero, since we subtract the "zero" level from the signal (i.e., $1/\tau_0$ from $1/\tau$). The confidence level for the LOD calculation was stated on lines 25, 445, 446, and 448 as (1 s, 1 σ); from this, it is straightforward to calculate the LOD by multiplying with the k value of one's choice. However, the reviewer is correct that we should have been more careful here since $k = 2$ or $k = 3$ are more commonly chosen. In response to the reviewer's comments, we have changed the definitions on these lines to (1 s, 2 σ) and adjusted all values accordingly.

2. The authors have taken the "LOD" for the CRDS of 87 ppt (1 sigma, 1 s) and divided by the CL of 69 to come up with the LOD for PANs of 1.3 ppt. Realistically, measuring PANs involves measuring NO2 twice in amplification mode and in reference mode (either sequentially in a single channel instrument, or simultaneously with in a multi-channel instrument), so there should probably be another factor of sqrt(2).

Our apologies as we should have stated how the calculation was made. The statistics we stated are based on time series after subtraction of the reference channel, making multiplication by another factor of $\sqrt{2}$ unnecessary. We inserted the following on line 448:

"... LOD for Σ PAN* (calculated on the basis of observed precision after subtraction of the reference channel signal, multiplying by $\sqrt{2}$, and dividing this precision by the CL) was ..."

We also noted that the precision can vary slightly between days and detection channels and added the following on line 444:

"The precision of the NO₂ measurement (and hence the LOD) varied slightly between detection channels and from day to day. Typically, when sampling zero air, the LOD for NO₂ was ~~~100 pptv~~47 pptv (1 s, ~~2~~1 σ 1- σ)."

Also, the authors point out that the precision of the CRDS NO2 measurement is affected by the presence of NO and ethane reagent gases. For measurement in ambient air, or laboratory air, what is the precision of measuring NO2?

We have only determined the precision under laboratory conditions and stated on line 445 that "In the presence of NO and ethane reagent gases, the LOD ~~increases to~~was larger, typically ~~~174 pptv~~87 pptv (1 s, ~~2~~ σ 1- σ)."

In ambient air, NO₂ and O₃ concentrations vary naturally; the extent of these fluctuations depend on the measurement location. We use parallel detection channels to keep track of (most of) such changes, but we agree that this could still be a source of additional noise. In addition, there may be noise associated with locating the instrument at a field site, where power, temperature, etc. can fluctuate. We have added the following statement on line 452:

"Under field conditions, where NO, NO₂ and O₃ concentration vary, the LOD is expected to be higher, though this was not evaluated in this work."

The LOD (and precision) for an actual PNs measurement in ambient air would be affected by the precision of the CRDS NO₂ measurement at the actual measurement conditions. For example, if O₃ is 25 ppb, some portion of the O₃ will react with the NO to give up to 25 ppb NO₂ – is the precision the same at 0 ppb and 25 ppb? This has likely been addressed in earlier NO₂ CRDS papers but should be mentioned for the reader's sake.

Please see our response to the preceding comment.

Mihele, C. M., and Hastie, D. R.: Optimized operation and calibration procedures for radical amplifier-type detectors, Journal Of Atmospheric And Oceanic Technology, 17, 788-794, 10.1175/1520-0426(2000)017<0788:OOACPF>2.0.CO;2, 2000.

Paul, D., Furgeson, A., and Osthoff, H. D.: Measurement of total alkyl and peroxy nitrates by thermal decomposition cavity ring-down spectroscopy, Rev. Sci. Instrum., 80, 114101, 10.1063/1.3258204 2009.

Taha, Y. M., Saowapon, M. T., and Osthoff, H. D.: Detection of triacetone triperoxide by thermal decomposition peroxy radical chemical amplification coupled to cavity ring-down spectroscopy, Anal. Bioanal. Chem., 10.1007/s00216-018-1072-0, 2018.

Quantification of peroxyntiric acid and peroxyacyl nitrates using an ethane-based thermal dissociation peroxy radical chemical amplification cavity ring-down spectrometer

5 Youssef M. Taha¹, Matthew T. Saowapon¹, Faisal V. Assad¹, Connie Z. Ye¹, Xining Chen^{1,a}, Natasha M. Garner¹, and Hans D. Osthoff¹

¹ Department of Chemistry, University of Calgary, 2500 University Drive N.W., Calgary, Alberta, Canada T2N 1N4

^a now at: Department of Chemistry, McGill University, 801 Sherbrooke St. West, Montreal, Quebec, Canada H3A 2K6

Correspondence to: Hans D. Osthoff (hosthoff@ucalgary.ca)

Abstract. Peroxy and peroxyacyl nitrates (PNs and PANs) are important trace gas constituents of the troposphere which are challenging to quantify by differential thermal dissociation with NO₂ detection in polluted (i.e., high-NO_x) environments. In this paper, a thermal dissociation peroxy radical chemical amplification cavity ring-down spectrometer (TD-PERCA-CRDS) for sensitive and selective quantification of total peroxy nitrates ($\Sigma\text{PN} = \Sigma\text{RO}_2\text{NO}_2$) and of total peroxyacyl nitrates ($\Sigma\text{PAN} = \Sigma\text{RC}(\text{O})\text{O}_2\text{NO}_2$) is described. The instrument features multiple detection channels to monitor the NO₂ background and the RO_x (= HO₂ + RO₂ + ΣRO_2) radicals generated by TD of ΣPN and/or ΣPAN . Chemical amplification is achieved through addition of 0.6 ppm NO and 1.6% C₂H₆ to the inlet. The instrument's performance was evaluated using peroxyntiric acid (PNA) and peroxyacetic or peroxypropionic nitric anhydride (PAN or PPN) as representative examples of ΣPN and ΣPAN , respectively, whose abundances were verified by iodide chemical ionization mass spectrometry (CIMS). The amplification factor or chain length increases with temperature up to 69±5 and decreases with analyte concentration and relative humidity (RH). At inlet temperatures above 120 °C and 250 °C, respectively, PNA and ΣPAN fully dissociated, though their TD profiles partially overlap. Furthermore, interference from ozone (O₃) was observed at temperatures above 150 °C, rationalized by its partial dissociation to O atoms which react with C₂H₆ to form C₂H₅ and OH radicals. Quantification of PNA and ΣPAN in laboratory-generated mixtures containing O₃ was achieved by simultaneously monitoring the TD-PERCA responses in multiple parallel CRDS channels set to different temperatures in the 60 °C to 130 °C range. The (1 s, $\pm 2\sigma$) limit of detection (LOD) of TD-PERCA-CRDS is ~~3.46.8~~ pptv for PNA and ~~1.32.6~~ pptv for ΣPAN and significantly lower than TD-CRDS without chemical amplification. The feasibility of TD-PERCA-CRDS for ambient air measurements is discussed.

1 Introduction

30 The RO_x ($= \text{OH} + \text{HO}_2 + \Sigma \text{RO}_2$) radicals and the nitrogen oxides ($\text{NO}_x = \text{NO} + \text{NO}_2$) are important trace constituents of the atmosphere that drive diverse processes such as the photochemical production of ozone (O_3) in the troposphere (Kirchner and Stockwell, 1996; Fleming et al., 2006), the catalytic destruction of O_3 in the stratosphere (Bates and Nicolet, 1950; Stenke and Grewe, 2005; Solomon, 1999; Portmann et al., 1999), and the chemistry of organic aerosol formation (Ziemann and Atkinson, 2012; Ehn et al., 2014; Crouse et al., 2013). In the troposphere, 35 the concentrations of these species are frequently buffered by RO_x and NO_x reservoir species, of which peroxyacetic acid (PNA, HO_2NO_2), alkyl peroxy nitrates such as methyl peroxy nitrate ($\text{CH}_3\text{O}_2\text{NO}_2$, MPN), and the peroxyacyl nitrates (PANs, $\text{RC}(\text{O})\text{O}_2\text{NO}_2$) are important examples (Singh et al., 1992; Roberts, 1990). Much insight into RO_x and NO_x chemistry has been gained by measuring the atmospheric abundances of these reservoirs. Significant PNA concentrations, for example, have been observed in the polar regions (Slusher et al., 2001; Davis et al., 2004; Jones et al., 2014), aloft in the free and upper troposphere (Kim et al., 2007; Murphy et al., 2004), in highly polluted environments such as the Uintah basin in winter (Veres et al., 2015), and in urban atmospheres (Spencer et al., 2009; Chen et al., 2017a), and have given valuable insights into radical budgets at these locations. The PANs and PNA are prone to thermal dissociation, such that higher concentrations are more commonly observed in cold regions, aloft in the free / upper troposphere, or in winter (Table 1). On the other hand, their rate of production is 45 greater in summer as the actinic flux intensifies. Mixing ratios of PNA peak in the range from ~~10s-tens~~ to a few ~~100s-hundreds~~ of parts-per-trillion by volume (pptv, 10^{-12}) and those of peroxyacetic nitric anhydride (PAN; $\text{CH}_3\text{C}(\text{O})\text{O}_2\text{NO}_2$) can exceed ten parts-per-billion by volume (ppbv, 10^{-9}) (Tuazon et al., 1981).

There is ongoing interest to develop improved techniques for quantification of PANs (Roberts, 2007; Wooldridge et al., 2010; Zheng et al., 2011; Tokarek et al., 2014) and PNA (Murphy et al., 2004; Spencer et al., 2009; Veres et al., 2015; Chen et al., 2017a). Thermal dissociation (TD) methods (Table 2) such as TD coupled to laser-induced 50 fluorescence (TD-LIF) (Wooldridge et al., 2010; Day et al., 2002; Di Carlo et al., 2013), to cavity ring-down spectroscopy (TD-CRDS) (Paul et al., 2009; Thaler et al., 2011; Paul and Osthoff, 2010; Thieser et al., 2016; Sobanski et al., 2016; Womack et al., 2017), or to cavity phase-shift spectroscopy (TD-CAPS) (Sadanaga et al., 2016) detection of NO_2 are attractive as they can be used to monitor all components of odd nitrogen (NO_y) in 55 parallel, including NO_2 (inlet operated at ambient temperature), total peroxy nitrates ($\Sigma \text{PN} = \text{PNA} + \text{MPN} + \dots$; inlet heated to ~ 100 °C), total peroxyacyl nitrates ($\Sigma \text{PAN} = \text{PAN} + \text{peroxypropionic nitric anhydride}$ ($\text{C}_2\text{H}_5\text{C}(\text{O})\text{O}_2\text{NO}_2 + \dots$; ~ 250 °C), total alkyl nitrates + ClNO_2 (ΣAN ; ~ 420 °C), and HNO_3 (~ 600 °C), simply by

deploying multiple detection channels and setting appropriate inlet temperatures. Molecules such as NO and HONO can be quantified through addition of O₃ following TD (Wild et al., 2014; Womack et al., 2017; Fuchs et al., 2009).

60 When used in polluted (i.e., high-NO_x) environments, however, a drawback of the TD methods is that quantification of ΣPN (and, to a lesser degree, also of ΣPAN) is compromised because of the large error introduced from subtraction of the NO₂ background, which is often 2 – 4 orders of magnitudes larger than the ΣPN abundance. In such high-NO_x environments, on the other hand, mixing ratios of RO_x radicals are generally much smaller, < 100 pptv (Wood et al., 2016), than those of NO₂, such that a better strategy may be to quantify the peroxy and

65 peroxyacyl radicals generated in stoichiometric amounts during TD of ΣPN and/or ΣPAN rather than NO₂. The RO_x radicals may be quantified by chemical ionization mass spectrometry (CIMS) (Hanke et al., 2002; Edwards et al., 2003; Chen et al., 2004; Slusher et al., 2004; Hornbrook et al., 2011); in fact, a TD-CIMS method has been developed to quantify PAN by titrating the peroxyacetyl radical with iodide reagent ion (Slusher et al., 2004). Other RO_x radical detection methods include LIF (Faloona et al., 2004; Heard, 2006; Fuchs et al., 2008;

70 Dusanter et al., 2009) and peroxy radical chemical amplification (PERCA) coupled to NO₂ detection (Cantrell et al., 1984; Hastie et al., 1991; Green et al., 2006; Liu and Zhang, 2014; Horstjann et al., 2014). The PERCA method is attractive as it allows the infrastructure of existing TD instruments with NO₂ detection to be utilized. In PERCA coupled to NO₂ detection, concentrations of RO_x radicals are amplified by factors of between ~20 to ~190 through a series of catalytic reactions, usually involving parts-per-million by volume (ppmv, 10⁻⁶) mixing

75 ratios of nitric oxide (NO) and percent levels of either carbon monoxide (CO) (Cantrell et al., 1984) or a short chain hydrocarbon such as ethane (C₂H₆) (Mihele and Hastie, 2000; Wood et al., 2016) (R1-R6, [Table 2](#)[Table 3](#)). Under these conditions, the peroxy radicals catalytically convert NO to NO₂, and the amount of NO₂ produced over a constant reaction period is proportional to the number of radicals that were present originally.

The measurement of peroxy radicals by PERCA is prone to [matrix effects and](#) interferences. For instance, a key

80 operational parameter of any PERCA instrument is the radical chain length or amplification factor (CL), which must be carefully calibrated. This chain length is suppressed by water vapour, whose presence increases the rates of radical loss on the inner walls of the PERCA chamber and the rates of certain gas-phase reactions, e.g., the reaction between the hydroperoxyl radical - water dimer (HO₂·H₂O) with NO to peroxyxynitrous acid (HOONO) which isomerizes to nitric acid (HONO₂) (Mihele and Hastie, 1998; Mihele et al., 1999 ; Mihele and Hastie, 2000).

85 The most obvious way to minimize wall reactions and to prevent weakly bound clusters such as HO₂·H₂O from forming is to apply heat. When quantification of ambient RO_x radicals is the goal, this is avoided to prevent TD of ΣPN or ΣPAN (which are more abundant than free RO_x radicals). [TD of ΣPN or ΣPAN produces radicals that as these molecules would](#) interfere [with the measurement of free RO_x radicals](#) (Mihele and Hastie, 2000). On the other

hand, if measurement of Σ PN or Σ PAN is desired (such as in this paper), this interference is turned into a measurement principle. We are aware of only one prior attempt to quantify peroxy nitrates in this manner: Blanchard et al. thermally decomposed PAN eluting from a chromatographic column in the presence of NO and CO and quantified the amplified NO_2 using luminol chemiluminescence (Blanchard et al., 1993).

In this manuscript, we probe the feasibility of selectively quantifying Σ PN and Σ PAN through their respective peroxy radical TD fragments by thermal decomposition peroxy radical chemical amplification cavity ring-down spectroscopy (TD-PERCA-CRDS). The instrument uses a 405 nm blue diode laser CRDS (Paul and Osthoff, 2010) to monitor NO_2 and the ethane-based chemical amplification scheme described by Wood et al. (2016), chosen because of ethane's lower toxicity compared to CO. Thermal dissociation profiles were determined for PAN, PPN, and PNA. Quantification of trace levels of PAN, PPN, and PNA by TD-PERCA-CRDS is demonstrated and compared to parallel measurements by iodide CIMS. The suitability of TD-PERCA-CRDS as a highly sensitive (sub-pptv) Σ PN and Σ PAN detection method for ambient measurements is discussed.

2 Experimental Section

2.1 TD-PERCA-CRDS

2.1.1 Single-channel inlet

The majority of the experiments described in this manuscript were conducted using a single-channel TD-PERCA inlet that ~~has been described elsewhere~~ is described and depicted as [Figure S1 of the Electronic Supplementary Material of](#) (Taha et al., 2018). Briefly, NO in N_2 (100.2 ppmv, Scott-Marrin, Riverside, CA) was scrubbed of NO_2 by passing through iron(II) sulfate heptahydrate (99%, Sigma-Aldrich, Oakville, ON) prior to being combined with either a flow of N_2 gas (Praxair) or ethane (CP grade, 99%, Matheson, Baskin Ridge, NJ). The gas mixture was directed towards the 80-cm long PERCA chamber (1.27 cm or 1/2" outer diameter (o.d.)). When NO and N_2 were mixed prior to the PERCA chamber, a "PERCA off" signal was observed, and ethane was added after the PERCA chamber to maintain constant flow (and pressure) through the system. Conversely, when NO and ethane were directed towards the PERCA chamber a "PERCA on" signal was observed. To maintain flows and pressures through the system during "PERCA on" mode, N_2 was added to the inlet at an addition point after the PERCA chamber.

The inlet was connected to a four-channel CRDS described elsewhere (Odame-Ankrah, 2015). Briefly, concentrations of NO_2 were monitored via its absorption at 405 nm (Paul and Osthoff, 2010). A flow containing ppmv levels of O_3 in O_2 was added to one CRDS channel to monitor NO_x (Fuchs et al., 2009). [The remaining two](#)

channels were equipped with heated quartz tubes to monitor $\text{NO}_2 + \Sigma\text{PAN}$ and $\text{NO}_2 + \Sigma\text{PAN} + \text{total alkyl nitrates}$ (ΣAN) (Paul et al., 2009). Each channel was connected to a MFC set to a flow rate of ~ 0.84 slpm. All four CRDS

120 cells were connected to sample the gases exiting the single-channel TD-PERCA inlet, though in principle a single CRDS detection channel would have sufficed to carry out the measurements.

When radical free "zero" air was sampled with the single channel inlet, a negative offset (up to 1 ppbv) was observed when the 3-way solenoid valves were switched between PERCA "on" and "off" (data not shown). This artefact was not observed with the dual channel setup (section 2.1.2) and was not further investigated but may have
125 been caused by differences in the ethane flows through the needle valve induced by pressure changes (up to 15 Torr) during switching between PERCA on and off.

2.1.2 Dual-channel TD-PERCA-CRDS

Time resolution, signal-to-noise, and subtraction of background NO_2 can be significantly improved in a PERCA instrument by implementing dual detection channels where both amplified and background signals are
130 simultaneously monitored (Green et al., 2006; Cantrell et al., 1996). The dual channel TD-PERCA setup used in this work is shown in Figure 1. The NO reagent gas is added at the same flow rate and concentration as in the single-channel version near the tip of the inlet (after the zero air and calibration gas ports). The residence time prior to the ethane addition point (~ 2.0 s) suffices to destroy RO_x radicals (via reaction with NO) prior to chemical amplification. Addition of either NO or ethane is on/off modulated using 2-way normally-open valves connected
135 to a pump via $50 \mu\text{m}$ critical orifices (Lenox Laser, Glen Arm, MD) in a similar fashion as described earlier (Odame-Ankrah and Osthoff, 2011).

A portion of the sample flow of ~ 0.74 slpm was diverted prior to TD to monitor the "background" NO_2 concentration in one CRDS channel. The remaining flow (~ 2.2 slpm) was passed through the heated quartz tube and PERCA chamber as described earlier and sampled by the other three CRDS channels to monitor background
140 NO_2 plus the amplified NO_2 signal.

2.1.3 Four-channel differential temperature TD-PERCA-CRDS

An instrument with four identical measurement channels was set up to enable simultaneous quantification of NO_2 , $\text{NO}_2 + \Sigma\text{PN}$ and $\text{NO}_2 + \Sigma\text{PN} + \Sigma\text{PAN}$. This version was similar to dual channel setup described above and simply added two additional PERCA chambers; all three PERCA chambers were connected to separate CRDS channels.
145 The quartz PERCA chamber was replaced with three identical 1.27 cm (1/2") o.d. and 0.95 cm (3/8") i.d. fluorinated ethylene propylene (FEP) Teflon™ tubes externally heated using stretch-to-fit heaters (Watlow, St. Louis, MO) to

60, 80 and 100 °C, respectively. A common inlet filter was placed between the PERCA chambers and the ethane addition point. A flow restriction was placed ahead of the common filter to achieve a pressure of 380 - 400 Torr at a flow rate of 0.8 slpm per channel (total flow rate ~3.2 slpm).

150 **2.2 Synthesis and delivery of PAN and PPN**

The synthesis of PAN and PPN from their corresponding anhydrides was described earlier (Mielke and Osthoff, 2012; Furgeson et al., 2011). Aliquots in tridecane were stored in 2.0 mL centrifuge tubes (VWR) in a freezer until needed.

To separate PAN and PPN from impurities generated during synthesis and storage (i.e., NO₂, HNO₃ and alkyl
155 nitrates (Grosjean et al., 1994)), a preparatory scale GC setup (Figure 2) was used. First, the contents of two tubes containing PAN and PPN in tridecane were combined in a 3-valve glass vessel. This vessel was connected to a 2-position GC-Valve (VICI Valco EH4C10WE, Houston, TX) and mildly pressurized (~0.1 atm above ambient) using oxygen (Praxair) delivered through a 10 µm critical orifice. Two megabore capillary gas chromatography (GC) columns (Restek RTX-1701, 0.53 mm i.d., 1.00 µm film thickness, State College, PA) of equal lengths (3 m)
160 were connected to the ports adjacent to the one connected to the glass vessel. The outlet of one GC column was connected to the PERCA inlet, whereas the other was exhausted into a waste line. The port opposite to the glass vessel was also pressurized with oxygen such that both columns remained under flow at all times. Gases were delivered by switching the valve to position A (Figure 2) for ~40 s. The output of the preparatory-scale GC was diluted with ZA or air passed through a custom-built scrubber system to meet the sample flow requirements of the
165 TD-PERCA CRDS and/or CIMS. The relative humidity (RH) of the gases delivered was monitored using a temperature/RH probe (VWR) placed inline.

The preparatory scale GC setup allowed delivery of short "bursts" of PAN and PPN. To deliver a constant and low PAN concentration over prolonged time periods, air was drawn from a 4,000 L Teflon chamber, initially filled with scrubbed (i.e., PAN-free) air and to which the head space above a PAN/tridecane solution had been added. An
170 internal mixing fan ensured constant output.

2.3 Synthesis and delivery of PNA

2.3.1. Batch sample

A batch PNA sample was synthesized from reaction of nitronium tetrafluoroborate (NO₂BF₄; Sigma-Aldrich) with H₂O₂ as described by Chen et al. (2017a). Briefly, a 50% H₂O₂ solution (Sigma-Aldrich) was concentrated using a
175 gentle N₂ flow over a period of several days. A small aliquot (200 µL) of concentrated H₂O₂ was placed in a 3-

valve glass vessel cooled to 0 °C using an external circulating chiller, and 120 mg of NO₂BF₄ were added. The headspace of the glass vessel was flushed with a 50 sccm flow of N₂ delivered by a MFC. This flow delivered very high concentrations and contained substantial and variable amounts of impurities (mainly HNO₃), even when the vessel temperature was lowered to -20 °C. The batch sample was used to calibrate the CIMS against TD-CRDS (section 2.4).

2.3.2. Photolysis source

Gas flows containing low and reproducible concentrations of PNA were generated dynamically in a similar fashion to the method described by Veres et al. (2015) by combining the output of a HO₂ photochemical source with NO₂. Ultrapure N₂ (Praxair) was passed through a bubbler filled with deionized water at a flow rate of 100 sccm and combined with 2 sccm of O₂ (Praxair). This mixture was passed through a ¼" (0.635 cm) o.d. quartz tube partially illuminated by a low-pressure 185 nm mercury quartz lamp (Jelight 95-2100-2, Irvine, CA). This generated a mixture of O₃ (~30 ppbv after dilution), OH and HO₂, whose concentrations were controlled with a sliding metal sleeve (VWR) which modified the length of the quartz tubing that was illuminated. This flow was combined with between 4 and 16 ppmv NO₂ to yield a gas mixture containing PNA which was immediately (< 5 cm tube length) diluted with zero or scrubbed air flowing at a rate slightly greater than the amount sampled by the instruments. The NO₂ gas stream was generated by mixing between 1.4 and 3.0 sccm of NO (100.2 ppmv in N₂; Scott-Marrin, Riverside, CA) with a slightly less than stoichiometric amount of O₃ in ~20 sccm O₂, generated by illuminating O₂ with a low-pressure 254 nm mercury quartz lamp (Jelight). The amount of PNA delivered from this source was quantified by TD-CRDS.

2.4 Chemical ionization mass spectrometry

The CIMS and its operation have been described elsewhere (Mielke et al., 2011; Mielke and Osthoff, 2012; Abida et al., 2011). For measurements of PAN or PPN, the instrument was operated with iodide reagent in declustering mode (collisional dissociation chamber voltage = -24.7 V) and sampled through a short section of 1.27 cm (½") o.d. PFA Teflon™ tubing heated to 190 °C. The inlet flow was diluted with nitrogen saturated with water vapour to maintain a minimum RH of ~16% with the ion-molecule reaction region (IMR). PAN and PPN were quantified using the acetate and propionate ions (*m/z* 59 and 73). Ion counts were normalized to 10⁶ reagent ion counts prior to presentation. The instrument response factor for PAN was calibrated against TD-CRDS (Mielke and Osthoff, 2012) and was 11±3 Hz pptv⁻¹.

For PNA measurements, the CIMS was operated with an ambient temperature inlet and in clustering mode
205 (collisional dissociation chamber voltage = -8.9 V); under these conditions, $\sim 5 \times 10^5$ I⁻ and $\sim 2 \times 10^4$ I⁻·H₂O ions were
observed. Mixing ratios of PNA were monitored primarily using NO₃⁻ at *m/z* 62, which is formed via PNA
decomposition within the IMR (Abida et al., 2011). The HNO₃·I⁻ and HO₂NO₂·I⁻ clusters at *m/z* 190 and *m/z* 206
(Veres et al., 2015; Chen et al., 2017a) were also monitored.

The PNA response factors were determined using TD-CRDS (i.e., without added PERCA gases) with its inlet
210 operated at 120 °C (Figure 3). Assuming that one equivalent of NO₂ is generated for each PNA molecule thermally
dissociated, the CIMS response factors, normalized to 10⁶ I⁻ counts, were 34.7±0.2 Hz pptv⁻¹ and 0.023±0.002 Hz
pptv⁻¹ at *m/z* 62 and 206, respectively. These response factors are consistent with calibration factors by other groups
(Veres et al., 2015; Chen et al., 2017a), with the low response at *m/z* 206 rationalized by the low number of I⁻·H₂O
ions. Even though the CIMS response at *m/z* 62 is not specific (Abida et al., 2011), it was used in the laboratory
215 experiments presented here to monitor PNA rather than *m/z* 206 because of its larger response factor and thus
higher sensitivity.

2.5 Box model simulations

Box model simulations were carried out using a subset of the MCM V3.3.1 obtained from
<http://mcm.leeds.ac.uk/MCM> (Jenkin et al., 1997; Saunders et al., 2003; Jenkin et al., 2012) and the Kinetic
220 Preprocessor (KPP) (Sandu and Sander, 2006) to aid in the interpretation of observations. Details are given in the
S.I.

3 Results

3.1 Thermal dissociation profiles

The TD profiles of PNA, PAN, and PPN were measured by TD-CRDS (i.e., without amplification) with the single-
225 channel inlet and are shown in Figure 4. The superimposed trend lines are simulations based on the TD model
introduced by Paul et al. (2009) and the Arrhenius parameters in ~~Table 3~~[Table 4](#) and are consistent with the
observations. The TD profiles of PNA and PAN/PPN partially overlap and are consistent with the 5%/95% ranges
given in Figure 3 of Wooldridge et al. (2010). PNA and PAN or PPN fully dissociated at temperatures of 120 °C
and 250 °C, respectively. These temperatures were used in subsequent experiments when complete dissociation of
230 either PNA or PAN/PPN was desired.

Also shown in Figure 4 is the TD-PERCA-CRDS signal observed when sampling O₃, an interfering species (see section 3.6.1).

3.2 Measurement of PAN and PPN by TD-PERCA-CRDS

235 A time series demonstrating amplification of PAN and PPN in the TD-PERCA-CRDS ~~operated with its inlet at 250 °C~~ is shown in Figure 5. In this experiment, PAN and PPN were delivered via the preparatory-scale GC (Figure 2), and the single-channel setup (section 2.1.1) was used.

PAN and PPN eluted from the GC column after 3 min and 6 min, respectively. The compounds eluted as plateaus because of the relatively long (~30 s) injection time. In Figure 5A, PAN and PPN are observed only by the heated (NO₂+ ΣPAN) TD-CRDS channel. This channel was operated with its quartz inlet at 250 °C, where they to
240 quantitatively (see Figure 5 of (Paul et al., 2009)) decompose PAN and PPN to NO₂. at-In this example, mixing ratios of 2.00±0.09 ppbv and 1.86±0.12 ppbv were observed, respectively (errors are 1 σ of 1 s data). After the PERCA heater was set to 250 °C as well, similar amounts of NO₂, 2.04±0.09 ppbv and 1.97±0.12 ppbv, were observed in the ambient temperature channel for PAN and PPN, respectively. Marginally higher amounts were observed in the heated CRDS channel (2.42±0.10 and 2.06±0.14 ppbv) (Figure 5B). The lower amounts observed
245 in the unheated CRDS channel result from recombination of peroxyacyl radicals with NO₂ (mostly in the unheated PERCA chamber), which suppresses the signal in the unheated CRDS channel but not in the heated one. Hence, the NO₂ + ΣPAN data are a more accurate measure of the PAN and PPN concentrations delivered.

Because PAN and PPN dissociate with 1:1 stoichiometry, the amount of peroxyacyl radicals produced during thermal dissociation is the same as the amount of NO₂ generated. When ~0.75 ppmv of NO was added (Figure 5C),
250 the peroxyacyl and, subsequently, the methyl (or ethyl) peroxy, and the hydroperoxyl radicals oxidize NO to NO₂ (reactions R8/R10, R1/R5, and R3; ~~Table 2~~Table 3) and the NO₂ signal relative to the signal obtained in the absence of NO is amplified by a factor of four. The ratios observed (Figure 5C relative to Figure 5B) were 4.0±0.2 and 3.8±0.3 for PAN and PPN, respectively, and are consistent with earlier observations at lower NO mixing ratios (i.e., Figure 6 of Paul and Osthoff (2010)).

255 Next, NO and ethane were added at mixing ratios (0.75 ppmv NO and 1.5% C₂H₆) that Wood et al. (2016) determined to be optimal for ambient temperature PERCA. Under these conditions, the signals amplified to 116.0±1.3 ppbv and 109.3±0.7 ppbv (Figure 5D), corresponding to CLs (relative to Figure 4B) of 48±2 and 53±4 for PAN and PPN, respectively.

In the presence of ethane, marginally lower NO₂ concentrations (98.7% and 98.1%) were observed in the heated, NO₂ + ΣPAN TD-CRDS channel (compared to the absence of ethane). Partial scrubbing of NO₂ in heated quartz cells has been anecdotally observed in our group's and also others' (Womack et al., 2016) TD instruments; this effect varies between quartz cells and with sample history. Since the effect was relatively minor, it was neglected in this work.

3.3 Optimization of TD-PERCA amplification factors

Sequences, such as the one shown in Figure 5, were used to determine conditions leading to optimum amplification factors. The largest amplification factors were obtained with an ethane mixing ratio of ~1.6% - 1.7% (data not shown).

Figure 6 shows how the chain length varies with NO mixing ratio. In the absence of ethane, amplification factors of ~4 were observed (Figure 6, open symbols), consistent with the results shown in Figure 5C. When 1.7% ethane were added, the amplification factor increased with NO mixing ratio up to a maximum at 550±150 ppbv and then decreased, qualitatively consistent with the results reported by Wood et al. (2016).

The amplification factors shown in Figure 6 were slightly larger for PAN than for PPN mainly because the PPN mixing ratio of ~1.3 ppbv exceeded the optimum concentration range for PERCA (see section 3.5.2).

3.4 Parallel measurement of PNA by TD-PERCA-CRDS and CIMS

A sample time series showing TD-PERCA-CRDS measurements of photochemically generated PNA in scrubbed air is presented in Figure 7. Here, the TD-PERCA-CRDS was operated with the dual channel inlet (Figure 1) at 120 °C and with 1.6% C₂H₆ and 316±3 ppbv of NO (suboptimal NO mixing ratios). Figure 7A shows the NO₂ mixing ratios in the reference, NO₂ channel (~~grey-green~~ trace) and in the TD-PERCA-CRDS channel (~~green-grey~~ trace). In this example, the mixing ratio of PNA was changed approximately every 2 min by moving a sliding cover within the photochemical source.

The difference between these two signals is displayed in Figure 7B (red trace, left-hand axis). Superimposed in Figure 7B (right-hand axis) are the CIMS responses at *m/z* 62 (NO₃⁻), *m/z* 206 (HNO₄·I, multiplied by a factor of 100 for clarity), and *m/z* 190 (HNO₃·I).

The photochemical source co-generates OH which is lost on the inner walls of the quartz tubing or is titrated by NO₂ or ~~(to lesser extent since less abundant)~~ NO to HNO₃ or HONO, respectively. Conceivably, the co-generation of HNO₃ could interfere with quantification of PNA by CIMS at *m/z* 62. However, when the photolysis source was turned off at ~19:59 (Figure 7), HNO₃ was still observed for some time after at *m/z* 190 due to slow desorption

from the inner walls of the connecting tubing, whereas the ion counts at m/z 62 quickly (< 10 s) returned to background values close to zero Hz, indicating that the contribution of HNO_3 to ion counts at m/z 62 was negligible.

290 The scatter plot of the TD-PERCA-CRDS and CIMS data at m/z 62, multiplied by the CIMS response factor determined in Figure 3A, is shown in Figure 8A as dark blue circles. The signals by the two instruments are highly correlated ($r^2 = 0.979$), consistent with both instruments measuring the same molecule, PNA. The slope of this plot (26.3 ± 0.4) equals to the TD-PERCA-CRDS amplification factor for PNA. In contrast, the scatter plot of TD-PERCA-CRDS with the CIMS response at m/z 206 was unusable because of the latter's poor signal to noise ratio

295 (Figure 3B).

3.5 Factors affecting amplification factors

The amplification factor for PNA shown in Figure 8A is less than observed for PAN in Figure 8B and for PAN and PPN under optimal conditions (Figure 6). Though in this particular example the lower amplification factor was due to the less than optimal amount of NO added, lower amplification factors for PNA than for PAN were generally

300 observed, even when optimum NO mixing ratios were used.

The obvious difference is that different radicals, HO_2 in the case of PNA and a peroxyacyl radical ($\text{RC}(\text{O})\text{O}_2$) in the case of PAN or PPN, are generated initially. However, in both cases, the HO_2/HO radical pair is the main carrier of the amplification, such that this initial difference should only have a marginal effect. Wood et al. (2016) estimated the uncertainty arising from the range in peroxy radical reactivity to $\pm 9\%$.

305 Experimental parameters that can affect the amplification factor include relative humidity, radical concentration, and the PERCA inlet temperature; these factors are probed separately in the following sections. In each case, box model simulations were carried out (see S.I.) to aid in the interpretation of the data.

3.5.1 Dependence of chain lengths on relative humidity

We repeated the experiment described in section 3.4 with the scrubbed air humidified to 75% RH by passing the

310 make-up air through a bubbler. The resulting scatter plot is superimposed in Figure 8A as red squares. Indeed, the amplification factor for PNA was lowered from 26.3 ± 0.4 to 18.0 ± 0.2 when the RH was increased from 20% to 75%. Following these observations, the RH dependence was investigated systematically at constant NO and ethane concentrations -with TD-PERCA-CRDS operated under optimal conditions and with PAN and PPN at 250 °C inlet temperature. The results are summarized in Figure 9.

315 The amplification factor decreased by $(2.0 \pm 0.6)\%$ for every 10% increase in RH. This RH dependence is less than reported for ambient temperature PERCA: Between a RH of 0% and 50%, for example, the response of room

temperature PERCA dropped by 30% (Wood et al., 2016), whereas that of TD-PERCA decreased by 15%. A reduced RH dependence is expected as the elevated temperature suppresses formation of HO₂-H₂O (Kanno et al., 2006), whose reaction with NO is a major radical sink (Mihele and Hastie, 1998; Mihele et al., 1999 ; Mihele and Hastie, 2000). This interpretation is supported by box model simulations, which show a reduced RH dependence of the CL at higher temperatures (Figure S-4). In addition, we speculate that reactions of radicals on the inner walls of PERCA tubing are reduced at higher inlet temperature.

3.5.2 Dependence of chain lengths on radical concentration: dynamic range

It is well known in the PERCA community that the chain lengths decrease at high radical concentrations due to radical-radical reactions. Figures 8A and 8B demonstrate that the response of TD-PERCA-CRDS is linear for both PNA and PAN/PPN at low, atmospherically relevant mixing ratios (i.e., below ~~~0.6 ppbv~~600 pptv). The linear dynamic range is similar for PNA and PAN and PPN since the radical chain carriers are the same for both.

Figure 10 summarizes the PERCA responses as functions at larger PAN/PPN mixing ratios. –The largest amplification factor, 69±5, was observed when the TD-PERCA inlet was operated at 250 °C with PAN or PPN mixing ratios ≤ ~~600 pptv~~0.6 ppbv. Shorter chain lengths were observed at higher mixing ratios (e.g., 62±2 at ~~1.3 ppbv~~1300 pptv, 53±4 at ~~2.1 ppbv~~2100 pptv, and 48±2 at ~~2.4 ppbv~~2400 pptv, respectively). Thus, the amplification factor is concentration dependent at RO₂ mixing ratios above ~~600 pptv~~0.6 ppbv and is constant under atmospherically relevant trace conditions.

PERCA reactors utilizing CO as a chain carrier show non-linearity at RO₂ mixing ratios above ~200 pptv (Hastie et al., 1991), while room temperature ethane based PERCA have a reported linear dynamic range up to ~800 pptv (Wood et al., 2016). The greater dynamic range with ethane arises because of lower chain lengths and radical concentrations in the reactor and hence reduced radical-radical termination reactions (Wood et al., 2016). The linear range of the ethane TD-PERCA reactor of ~600 pptv falls in between these two extremes, as the CL and radical concentrations are greater than ethane PERCA at room temperature but less than those achievable with CO PERCA. The linear range observed is consistent with box model simulations, in particular when wall loss reactions are taken into account (Figure S-6).

3.5.3 Dependence of chain lengths on inlet temperature

Next, we investigated the temperature dependence of the TD-PERCA-CRDS signal when sampling photochemically generated PNA at constant RH and PNA mixing ratio. Figure 11 shows such a temperature scan

345 of ~180 pptv PNA (measured in parallel by CIMS). The non-amplified TD profile observed by TD-CRDS is superimposed for comparison.

A striking feature in Figure 11 is the very large increase in the amplified NO₂ signal observed at temperatures above ~150 °C. This is an artefact that arises from O₃ co-emitted by the photochemical source and is commented on further in section 3.6.1.

350 It is obvious from Figure 11 that the amplification factor is strongly dependent on temperature: Even though PNA fully dissociates at temperatures > ~90 °C in our inlets (Figure 4), the amplified signal increases by ~60% in the region from 90 °C to 135 °C (Figure 11, insert), corresponding to amplification factors of ~15 and ~22, respectively. This increase is qualitatively consistent (if extrapolated) with the higher amplification factor observed with PAN or PPN at 250 °C.

355 Box model simulations using only gas-phase chemistry from the MCM V3.3.1 (Figure S-3) show that the CL is expected to decrease with increasing temperature, opposite to what is observed. This occurs in the model because the chain-carrying reactions of HO₂ and RO₂ with NO (e.g., R3, [Table 2](#)~~Table 3~~) have negative activation energies and are hence slower at higher temperatures, yielding a lower CL at higher temperature. This is partially offset when the chemistry of HO₂·H₂O is added to the mechanism (Figures S-4 and S-5) but does not suffice to achieve
360 a higher CL at higher temperature; the latter is only predicted by the box model simulations if much lower wall loss reactivity of OH and HO₂ are assumed (see S1.3 and S1.4).

3.6 Interferences

3.6.1 Interference from O₃ in the measurement of ΣPAN at 250 °C

When sampling ambient air (data not shown) or when sampling photochemically generated PNA (Figure 11) the
365 amplified NO₂ increases sharply at PERCA inlet temperatures above ~150 °C. These observations can be rationalized by thermal decomposition of O₃. Even though only a small fraction of O₃ dissociates to O₂ + O at ~150 °C in the TD inlet (~0.1%; Figure 5 (Jones and Davidson, 1962; Heimerl and Coffee, 1979)), a comparatively large signal is generated because the O atom reacts with C₂H₆ to form two radicals, OH and C₂H₅ (Baulch et al., 1994). This reaction is competitive in the PERCA inlet (compared to reaction of O with O₂) because of the high C₂H₆
370 concentration (1.7%): The lifetime of O with respect to reaction with C₂H₆ is ~0.34 ms, which is of similar magnitude as the expected lifetime of O with respect to reaction with O₂ of ~0.15 ms (Hippler et al., 1990).

We considered an alternate inlet configuration in which the inlet length between the NO and ethane addition points is increased to allow for sufficient residence time completely titrate O₃ with the added NO. However, at the optimum NO mixing ratio for PERCA, the 1/e lifetime of O₃ is ~6 s, making this approach unfeasible.

375 Hence, if O₃ is sampled with an ethane-based TD-PERCA instrument heated above 150 °C, radicals are generated that are amplified by PERCA. Since O₃ is typically present at mixing ratios in the tens of ppbv in ambient air, quantification of ΣPAN with an ethane-based TD-PERCA-CRDS would be challenging. In contrast, TD-PERCA instruments using CO will not have this limitation, as CO reacts with O to CO₂ and would not generate RO_x radicals.

380 3.6.2 Interference from peroxyacetic acid in the measurement of ΣPAN at 250 °C

In a previous paper (Taha et al., 2018), we reported interference from peroxyacetic acid (PAA) when the inlet was operated at 250 °C. However, the mixing ratios delivered on those experiments were well above what is expected in ambient air. Further, it is unclear what fraction of PAA dissociates at 250 °C, since the Arrhenius parameters for TD of PAA are uncertain (~~Table 3~~ [Table 4](#)). Regardless of whose Arrhenius parameters are assumed, the
385 temperature needed to dissociate 0.1% of PAA is greater than that needed to dissociate 99.9% of PAN (~~Table 3~~ [Table 4](#)). In ambient air, PAA is present at concentrations of up to one order of magnitude greater than that of PAN (Phillips et al., 2013). We estimate that under typical conditions, the interference from PAA dissociation is <1% and likely be completely prevented if the inlet is operated at a temperature below 250 °C.

3.6.3 Interference from ΣPAN in the measurement of ΣPN at 95 °C – 110 °C

390 A temperature of 95°C (110 °C) is required to dissociate >90% (>99.9%) of PNA in the TD-PERCA inlet; at these temperatures, ~12% (~39%) of PAN dissociates (Figure 4). Since [PAN] > [PNA] (Table 1) and hence ΣPAN > ΣPN in most environments, the contribution of ΣPAN to the ΣPN signal in ambient air is substantial (and likely also variable given the slope of the PAN TD curve in this region). Hence, measurement of ΣPN in ambient air by TD-PERCA-CRDS with a single channel relative to an NO₂ background measurement is unfeasible.

395 3.7 Differential temperature TD-PERCA-CRDS for measurement of ΣPN and ΣPAN

3.7.1 Synthetic air mixtures

To overcome the limitations outlined in section 3.6, a multichannel, differential temperature approach was used. Here, two channels were operated at constant temperatures set in the 60 °C to 110 °C range to avoid the interference from O₃ dissociation and ensure that response for ΣPAN remains linear (by dissociating only a fraction of its

400 concentration). Since the amount of NO₂ generated by TD-PERCA is a function of temperature and radical chain length (CL_T) as well as a fraction dissociated (F_T) of PNA and ΣPAN, the responses in the two PERCA channels operated at different temperatures, T1 and T2, are:

$$[\text{NO}_2]_{\text{T1}} = \text{CL}_{\text{T1}} \times \text{F}_{\text{PAN,T1}} \times [\Sigma\text{PAN}] + \text{CL}_{\text{T1}} \times \text{F}_{\text{PNA,T1}} \times [\Sigma\text{PN}] + [\text{NO}_2]_{\text{ref}} \quad (1\text{a})$$

$$[\text{NO}_2]_{\text{T2}} = \text{CL}_{\text{T2}} \times \text{F}_{\text{PAN,T2}} \times [\Sigma\text{PAN}] + \text{CL}_{\text{T2}} \times \text{F}_{\text{PNA,T2}} \times [\Sigma\text{PN}] + [\text{NO}_2]_{\text{ref}} \quad (1\text{b})$$

405 If the CL_T and F_T values are measured at temperatures T1 and T2 independently (i.e., offline), and [NO₂]_{ref} is quantified in an unheated, parallel reference channel, the mixing ratios of ΣPN and ΣPAN can be calculated by rearranging equations (1a) and (1b):

$$[\Sigma\text{PAN}] = \frac{([\text{NO}_2]_{\text{T1}} - [\text{NO}_2]_{\text{ref}}) \times \text{CL}_{\text{T2}} \text{F}_{\text{PNA,T2}} - ([\text{NO}_2]_{\text{T2}} - [\text{NO}_2]_{\text{ref}}) \times \text{CL}_{\text{T1}} \text{F}_{\text{PNA,T1}}}{\text{CL}_{\text{T2}} \text{F}_{\text{PAN,T2}} \times \text{CL}_{\text{T1}} \text{F}_{\text{PAN,T1}} - \text{CL}_{\text{T2}} \text{F}_{\text{PAN,T2}} \times \text{CL}_{\text{T1}} \text{F}_{\text{PNA,T1}}} \quad (2\text{a})$$

$$[\Sigma\text{PN}] = \frac{([\text{NO}_2]_{\text{T2}} - [\text{NO}_2]_{\text{ref}}) - \text{CL}_{\text{T2}} \text{F}_{\text{PAN,T2}} \times [\Sigma\text{PAN}]}{\text{CL}_{\text{T2}} \text{F}_{\text{PNA,T2}}} \quad (2\text{b})$$

410 A time series demonstrating this approach using the four channel setup is presented in Figure 12A. Here, a constant mixing ratio of PNA (along with NO₂ and O₃ from the photolysis source) was added to the inlet between 21:44 and 21:55. At 21:48:30 and at 21:50:45, PAN was added via the GC pre-column. The product of CL and F for PAN and PNA at 110 °C, 80 °C, and 60 °C was determined offline and are summarized in [Table 4](#)[Table 5](#) and assumed for same for all ΣPN and ΣPAN species.

415 The time series of PNA and PAN mixing ratios derived from equations 2a and 2b are presented in Figure 12B. Consistent results were obtained independent of which pair of channels was used in the calculations ([Table 5](#)[Table 6](#)).

3.7.2 Laboratory air

The differential temperature TD-PERCA-CRDS was then used to sample and determine ΣPN and ΣPAN in
420 laboratory air. The calibration parameters summarized in [Table 4](#)[Table 5](#) were used since they were determined with scrubbed air, which has the same RH as the air intake (i.e., the laboratory). The results are summarized in [Table 6](#)[Table 7](#).

The calculated room air ΣPN values mixing ratios are negative (i.e., not physically possible). On the other hand, the ΣPAN mixing ratios are unreasonably large as we have never observed similarly high mixing ratios in our
425 laboratory by GC, TD-CRDS, or by CIMS. Taken together, these observations suggest that there is (or are) species that dissociate in the TD inlet and generate RO_x radicals or, perhaps, atomic oxygen other than ΣPAN. These unknown interfering species seem to have different TD profiles than PAN and PNA as the differential response

differs when different pairs of channels are used in the calculation. Furthermore, the response to the unknown species is more prominent when the hottest (110 °C) channel is used in the calculation.

430 When ~260 pptv of PNA and ~480 pptv PAN (using the same setup as for Figure 12 and ~~Table 5~~ Table 6) were added to the sampled laboratory air, the responses (i.e., $\Delta(\Sigma\text{PN})$ and $\Delta(\Sigma\text{PAN})$) are consistent in all channels, which suggests that the chain lengths and dissociated fractions had not changed. This observation corroborates that the ethane based TD-PERCA-CRDS in reality quantifies ΣPAN^* , which includes PAN, PPN, etc. plus one or more unidentified species. In section 4, we speculate as to the potential identity of the interfering species.

435 3.8 Figures of merit

The ability of TD-PERCA-CRDS to detect radicals is limited by the instrument's ability to detect differences in NO_2 concentration after amplification, calculated using (Brown et al., 2002):

$$[\text{NO}_2]_{\min} = \frac{R_L}{c\sigma_{\text{NO}_2}} \left(\frac{\Delta\tau_{\min}}{\tau_0^2} \right) [\text{NO}_2]_{\min} = \frac{R_L}{c\sigma} \left(\frac{\Delta\tau_{\min}}{\tau_0^2} \right) \quad (3)$$

Here, $[\text{NO}_2]_{\min}$ is the smallest NO_2 concentration that can be detected, $\Delta\tau_{\min}$ is the smallest measurable difference
 440 between ring-down time constants in the presence (τ) and absence (τ_0) of NO_2 , c is the speed of light, σ_{NO_2} is the NO_2 absorption cross-section at 405 nm ($6.1 \times 10^{19} \text{ cm}^2 \text{ molecule}^{-1}$ (Paul and Osthoff, 2010)), and R_L is a correction factor. At the 1 σ level, $\Delta\tau_{\min}$ is approximately (Brown et al., 2002):

$$\Delta\tau_{\min} = \sqrt{2} \times \sigma(\tau_0) \quad (4)$$

The precision of the NO_2 measurement (and hence the LOD) varied slightly between detection channels and from
 445 day to day. Typically, ~~W~~ when sampling zero air, the LOD for NO_2 was ~~49~~ ~100 pptv (1 s, ~~1~~ 2 σ). In the presence of NO and ethane reagent gases, the LOD ~~increases~~ was larger, to ~~87~~ typically ~174 pptv (1 s, ~~1~~ 2 σ).

Employing the dual-channel-TD-PERCA-CRDS with the PERCA heater at 250 °C, a CL of 69 factored in, and in the absence of NO_2 , the (1 s, ~~1~~ 2 σ) LOD for ΣPAN^* (calculated on the basis of observed precision after subtraction of the reference channel signal, multiplying by $2\sqrt{2}$, and dividing this precision by the CL) was ~~1.32~~ 6 pptv. At an
 450 inlet temperature of 120 °C and with a CL of 26, the LOD for PNA was ~~3.46~~ 8 pptv. When averaging for 90 s, the minimum of an Allan variance plot (Figure 7 of Paul and Osthoff (2010)) the LOD ~~improves~~ improved to ~~8.71~~ 7 pptv for NO_2 -, ~~0.13~~ 26 pptv for ΣPAN^* , and ~~0.33~~ 66 pptv for PNA. Under field conditions, where NO, NO_2 and O_3 concentration vary, the LOD is expected to be higher, though this was not evaluated in this work.

455 The accuracy of TD-PERCA-CRDS is limited by uncertainties in CL ($\pm 7\%$ for dry air), variability in the response to different type of peroxy radicals ($\pm 9\%$) (Wood et al., 2016), and of the NO_2 measurement ($\pm 4\%$) which is dominated by uncertainties in the absorption cross-section and R_L (Paul and Osthoff, 2010). Adding these in quadrature gives a combined uncertainty of $\pm 12\%$ for dry air.

460 An additional uncertainty factor for the differential temperature TD-PERCA-CRDS is the uncertainty in F_T . The chambers are operated at temperatures where F_T is highly sensitive to temperature (Figure 4). Judging from the scatter observed (for example, in ~~Table 5~~Table 6), we estimate that an additional $\pm 5\%$ random error is introduced, raising the combined measurement uncertainty to $\pm 13\%$. Not included in this estimate are systematic errors that might arise from the unknown and potentially variable TD profile of the interferences included in ΣPAN^* .

4 Discussion

465 The main goal of this work was to evaluate the feasibility of using ethane-based TD-PERCA to quantify ΣPN and ΣPAN in ambient air. This work has identified several stumbling blocks that on aggregate insinuate that such a measurement would be difficult and error-prone in practice.

On the one hand, the ethane-based TD-PERCA-CRDS has demonstrated great LODs (< 1 pptv for ΣPAN^* and PNA). This constitutes a considerable improvement compared to our previous generation TD-CRDS, whose LOD was in the ~~100s-~~hundreds of pptv (Paul and Osthoff, 2010), and represents the first optical absorption measurement of PNA at concentration levels of the same magnitude as found in ambient air (Table 1). In addition, the measurement can tolerate a large NO_2 background through selective amplification of the desired signal: In Figure 12, for example, the NO_2 background was > 30 ppbv, yet PNA and PAN were quantified with a 1 s, 1 σ precision of < 6 pptv and < 40 pptv, respectively (~~Table 5~~Table 6). Moreover, the sensitivity of the ethane-based TD-PERCA is better than the room temperature measurement of RO_x radicals (1.6 pptv; 90 s, 2 σ) (Wood et al., 2016), mainly because of the greater amplification (~ 69 vs. ~ 25) and in spite of the CAPS sensor being slightly more sensitive to NO_2 than our CRDS. Furthermore, the instrument's sensitivity is comparable to (or better than) what is achievable with commonly used GC and CIMS methods. For example, at an inline temperature of 120°C , the sensitivity of TD-PERCA-CRDS for PNA was of the same order of magnitude as our CIMS at its non-specific ion at m/z 62 and the optimized CIMS recently described by Chen et al. (2017a).

480 The TD-PERCA-CRDS owes its good sensitivity to its high CL, which increases with temperature. Our attempts to rationalize the temperature through model simulations (see S.I.) were limited because models simulating PERCA need to take wall loss rates into account and are generally poor predictors of experimental chain lengths. From a

gas-phase kinetics perspective, reactions of HO₂ and RO₂ with NO (e.g., R3, [Table 2](#)[Table 3](#)) have a negative
485 activation energy and are thus expected to slow down at higher temperatures, decreasing turnover rates and the CL.
On the other hand, the RH dependence is reduced by heating, in part because one of the radical chain-terminating
reaction, HO₂+NO→HNO₃, proceeds via a water adduct (HO₂·H₂O) (Butkovskaya et al., 2007; Butkovskaya et al.,
2009). The temperatures within the PERCA reaction heater are sufficiently elevated to dissociate this intermediate,
shutting down this radical sink reaction. In addition, the elevated temperatures inside the reactor may lessen
490 reactions at the reactor inner wall surfaces (by driving off adsorbed water molecules, for example) though we lack
direct evidence for this happening.

On the other hand, however, the TD-PERCA-CRDS method has several drawbacks, some of which still need to be
overcome to make ambient measurements a reality.

The first challenge is posed by the TD profiles of PAN and PNA (Figure 4) which are not completely separated.
495 This overlap is particularly problematic in ambient air because the signal generated by the typically much smaller
PNA concentrations could be overshadowed by a much larger ΣPAN signal. In this work, the overlap of the TD
profiles of PNA and PAN (and, the rather limited dynamic range of <500 pptv) was overcome by the differential
temperature / linear combination method (section 3.7) in which ΣPAN was only partially dissociated and PNA
close to completely dissociated.

500 A complication is that methyl and ethyl peroxy nitrate have TD profiles that are similar, but not identical, to that
of PNA; these molecules dissociate at lower temperatures than PNA ([Table 3](#)[Table 4](#)). This does not matter if the
TD-PERCA inlets are operated at temperatures at which all three molecules are fully dissociated (or nearly so) as
in this work.

The differential temperature approach has the additional advantage of avoiding the O₃ interference that occurs
505 above 150 °C, which would otherwise have been a serious issue because of the typically much larger O₃ than PAN
or PNA concentrations in ambient air, and gave consistent results in synthesized air mixtures and room air.

A second drawback of TD-PERCA is the RH dependent CL, which necessitates frequent calibrations to determine
CL×F at each channel's temperature, though this could in principle be straightforward with photochemical sources
of PNA and PAN and automated switching. At the same time, frequent calibrations of CL and F would relax the
510 need to carefully match the responses in each of the TD channels, which is a requirement in conventional TD
instruments.

A third and most substantial drawback are the interferences. The O₃ interference is easily avoided by switching the
instrument from ethane to CO operation. With CO, any O generated from O₃ dissociation would react to form CO₂
and be of no further consequence. However, CO-PERCA is somewhat unappealing because of CO's high toxicity

515 and lack of smell, making its use impractical and impermissible in some university laboratories due to legitimate safety concerns. Mihele and Hastie (2000) used PAN as a radical source by heating a short section of the inlet of their CO-PERCA to 200 °C and found the CL to be the same as other radical sources (which included passing H₂ past a heated wire and a Cl₂ photolysis source), which suggests that the CL in a CO based PERCA is less dependent on temperature than with an ethane based PERCA, which would be another advantage of CO based PERCA.

520 The unknown interference observed in laboratory air is by far the biggest hurdle. We do not know the identity of the molecule or class of molecules interfering, and if the interference is present in ambient air, away from anthropogenic sources, or found only within a chemistry laboratory. We previously reported (Taha et al., 2018) that the ethane-based TD-PERCA-CRDS responds to peroxide explosives and also responds when sampling the head space above common skin cream and moisturizer products, which contain organosiloxanes. Organosiloxanes

525 have become ubiquitous in the environment and have been found in indoor air in ppbv levels (Rücker and Kümmerer, 2015). Their barriers to dissociation have been reported (Davidson and Thompson, 1971) and are too large for decomposition to occur at the inlet temperatures used in this work. However, Kulyk et al. (2016) recently suggested that pyrolysis of certain polysiloxanes may occur at temperatures as low as 70 °C. Clearly, more work is needed to identify which molecules or class of molecules interferes in TD-PERCA-CRDS and are included in

530 ΣPAN*. It is possible that the interfering species thermally dissociate(s) to release O atoms; if that's the case, this interference would not be present in a CO based TD-PERCA. Hence, measurements using a CO-based TD-PERCA should be attempted. Furthermore, such measurements should be complemented by parallel measurements of PNA, PAN and PPN by CIMS.

535 **Acknowledgments**

This work was made possible by the financial support of the National Science and Engineering Research Council of Canada (NSERC) in the form of a Discovery grant. The authors thank Ezra Wood for sharing a preprint version of a manuscript and useful discussions. YMT, CZY, and NMG acknowledge financial support from the NSERC Collaborative Research and Training Experience Program (CREATE) "Integrating Atmospheric Chemistry and
540 Physics from Earth to Space" (IACPES) and QEII graduate scholarships.

References

- 545 Abida, O., Mielke, L. H., and Osthoff, H. D.: Observation of gas-phase peroxyxynitrous and peroxyxynitric acid during the photolysis of nitrate in acidified frozen solutions, *Chem. Phys. Lett.*, 511, 187-192, 10.1016/j.cplett.2011.06.055 2011.
- Ahmadov, R., McKeen, S., Trainer, M., Banta, R., Brewer, A., Brown, S., Edwards, P. M., de Gouw, J. A., Frost, G. J., Gilman, J., Helmig, D., Johnson, B., Karion, A., Koss, A., Langford, A., Lerner, B., Olson, J., Oltmans, S.,
- 550 Peischl, J., Pétron, G., Pichugina, Y., Roberts, J. M., Ryerson, T., Schnell, R., Senff, C., Sweeney, C., Thompson, C., Veres, P. R., Warneke, C., Wild, R., Williams, E. J., Yuan, B., and Zamora, R.: Understanding high wintertime ozone pollution events in an oil- and natural gas-producing region of the western US, *Atmos. Chem. Phys.*, 15, 411-429, 10.5194/acp-15-411-2015, 2015.
- Atkinson, R., Baulch, D. L., Cox, R. A., Hampson, R. F., Kerr, J. A., Rossi, M. J., and Troe, J.: Evaluated kinetic,
- 555 photochemical and heterogeneous data for atmospheric chemistry .5. IUPAC Subcommittee on Gas Kinetic Data Evaluation for Atmospheric Chemistry, *Journal Of Physical And Chemical Reference Data*, 26, 521-1011, 10.1063/1.556011, 1997.
- Bates, D. R., and Nicolet, M.: The photochemistry of atmospheric water vapor, *J. Geophys. Res.*, 55, 301-327, 10.1029/JZ055i003p00301, 1950.
- 560 Baulch, D. L., Cobos, C. J., Cox, R. A., Frank, P., Hayman, G., Just, T., Kerr, J. A., Murrells, T., Pilling, M. J., Troe, J., Walker, R. W., and Warnatz, J.: Summary table of evaluated kinetic data for combustion modeling: Supplement 1, *Combustion and Flame*, 98, 59-79, 10.1016/0010-2180(94)90198-8, 1994.
- Blanchard, P., Shepson, P. B., Schiff, H. I., and Drummond, J. W.: Development of a gas-chromatograph for trace-level measurement of peroxyacetyl nitrate using chemical amplification, *Anal. Chem.*, 65, 2472-2477,
- 565 10.1021/ac00066a012, 1993.

- Brown, S. S., Stark, H., Ciciora, S. J., McLaughlin, R. J., and Ravishankara, A. R.: Simultaneous in situ detection of atmospheric NO_3 and N_2O_5 via cavity ring-down spectroscopy, *Rev. Sci. Instrum.*, 73, 3291-3301, 10.1063/1.1499214, 2002.
- 570 Butkovskaya, N., Kukui, A., and Le Bras, G.: HNO_3 forming channel of the HO_2+NO reaction as a function of pressure and temperature in the ranges of 72-600 Torr and 223-323 K, *J. Phys. Chem. A*, 111, 9047-9053, 10.1021/jp074117m, 2007.
- Butkovskaya, N., Rayez, M. T., Rayez, J. C., Kukui, A., and Le Bras, G.: Water Vapor Effect on the HNO_3 Yield in the $\text{HO}_2 + \text{NO}$ Reaction: Experimental and Theoretical Evidence, *J. Phys. Chem. A*, 113, 11327-11342, 10.1021/jp811428p, 2009.
- 575 Cantrell, C. A., Stedman, D. H., and Wendel, G. J.: Measurement of atmospheric peroxy-radicals by chemical amplification, *Anal. Chem.*, 56, 1496-1502, 10.1021/ac00272a065, 1984.
- Cantrell, C. A., Shetter, R. E., and Calvert, J. G.: Dual-inlet chemical amplifier for atmospheric peroxy radical measurements, *Anal. Chem.*, 68, 4194-4199, 10.1021/ac960639e, 1996.
- Chen, D. X., Huey, L. G., Tanner, D. J., Li, J. F., Ng, N. L., and Wang, Y. H.: Derivation of Hydroperoxyl Radical
580 Levels at an Urban Site via Measurement of Pernitric Acid by Iodide Chemical Ionization Mass Spectrometry, *Environm. Sci. Technol.*, 51, 3355-3363, 10.1021/acs.est.6b05169, 2017a.
- Chen, G., Davis, D., Crawford, J., Hutterli, L. M., Huey, L. G., Slusher, D., Mauldin, L., Eisele, F., Tanner, D., Dibb, J., Buhr, M., McConnell, J., Lefer, B., Shetter, R., Blake, D., Song, C. H., Lombardi, K., and Arnoldy, J.:
A reassessment of HOx South Pole chemistry based on observations recorded during ISCAT 2000, *Atmos.*
585 *Environm.*, 38, 5451-5461, 10.1016/j.atmosenv.2003.07.018, 2004.
- Chen, J., Wu, H., Liu, A. W., Hu, S. M., and Zhang, J.: Field Measurement of NO_2 and RNO_2 by Two-Channel Thermal Dissociation Cavity Ring Down Spectrometer, *Chin. J. Chem. Phys.*, 30, 493-498, 10.1063/1674-0068/30/cjcp1705084, 2017b.

Crouse, J. D., Nielsen, L. B., Jorgensen, S., Kjaergaard, H. G., and Wennberg, P. O.: Autoxidation of Organic
590 Compounds in the Atmosphere, *Journal of Physical Chemistry Letters*, 4, 3513-3520, 10.1021/jz4019207, 2013.

Davidson, I. M. T., and Thompson, J. F.: Dimethylsilanone from the pyrolysis of octamethylcyclotetrasiloxane,
Journal of the Chemical Society D: Chemical Communications, 251-252, 10.1039/c29710000251, 1971.

Davis, D., Chen, G., Buhr, M., Crawford, J., Lenschow, D., Lefer, B., Shetter, R., Eisele, F., Mauldin, L., and
Hogan, A.: South Pole NO_x chemistry: an assessment of factors controlling variability and absolute levels, *Atmos.*
605 *Environm.*, 38, 5375-5388, 10.1016/j.atmosenv.2004.04.039, 2004.

Day, D. A., Wooldridge, P. J., Dillon, M. B., Thornton, J. A., and Cohen, R. C.: A thermal dissociation laser-
induced fluorescence instrument for in situ detection of NO₂, peroxy nitrates, alkyl nitrates, and HNO₃, *J.*
Geophys. Res., 107, D6, 4046, 10.1029/2001JD000779, 2002.

Devush, S. S., Prisyazhnyuk, Z. P., and Kovalskaya, A. M.: Kinetics of the thermal gas-phase decomposition of
600 C1-C4 organic peracids, *Kinet. Catal.*, 24, 1098-1101, 1983.

Di Carlo, P., Aruffo, E., Busilacchio, M., Giammaria, F., Dari-Salisburgo, C., Biancofiore, F., Visconti, G., Lee,
J., Moller, S., Reeves, C. E., Bauguitte, S., Forster, G., Jones, R. L., and Ouyang, B.: Aircraft based four-channel
thermal dissociation laser induced fluorescence instrument for simultaneous measurements of NO₂, total peroxy
nitrate, total alkyl nitrate, and HNO₃, *Atmospheric Measurement Techniques*, 6, 971-980, 10.5194/amt-6-971-
605 2013, 2013.

Dusanter, S., Vimal, D., Stevens, P. S., Volkamer, R., and Molina, L. T.: Measurements of OH and HO₂
concentrations during the MCMA-2006 field campaign – Part 1: Deployment of the Indiana University laser-
induced fluorescence instrument, *Atmos. Chem. Phys.*, 9, 1665-1685, 10.5194/acp-9-1665-2009, 2009.

Edwards, G. D., Cantrell, C. A., Stephens, S., Hill, B., Goyea, O., Shetter, R. E., Mauldin, R. L., Kosciuch, E.,
610 Tanner, D. J., and Eisele, F. L.: Chemical ionization mass spectrometer instrument for the measurement of
tropospheric HO₂ and RO₂, *Anal. Chem.*, 75, 5317-5327, 10.1021/ac034402b, 2003.

- Ehn, M., Thornton, J. A., Kleist, E., Sipila, M., Junninen, H., Pullinen, I., Springer, M., Rubach, F., Tillmann, R., Lee, B., Lopez-Hilfiker, F., Andres, S., Acir, I.-H., Rissanen, M., Jokinen, T., Schobesberger, S., Kangasluoma, J., Kontkanen, J., Nieminen, T., Kurten, T., Nielsen, L. B., Jorgensen, S., Kjaergaard, H. G., Canagaratna, M., Maso, M. D., Berndt, T., Petaja, T., Wahner, A., Kerminen, V.-M., Kulmala, M., Worsnop, D. R., Wildt, J., and Mentel, T. F.: A large source of low-volatility secondary organic aerosol, *Nature*, 506, 476-479, 10.1038/nature13032, 2014.
- Eisele, F., Davis, D. D., Helmig, D., Oltmans, S. J., Neff, W., Huey, G., Tanner, D., Chen, G., Crawford, J., Arimoto, R., Buhr, M., Mauldin, L., Hutterli, M., Dibb, J., Blake, D., Brooks, S. B., Johnson, B., Roberts, J. M., Wang, Y. H., Tan, D., and Flocke, F.: Antarctic Tropospheric Chemistry Investigation (ANTCI) 2003 overview, *Atmospheric Environment*, 42, 2749-2761, 10.1016/j.atmosenv.2007.04.013, 2008.
- Faloona, I. C., Tan, D., Leshner, R. L., Hazen, N. L., Frame, C. L., Simpas, J. B., Harder, H., Martinez, M., Di Carlo, P., Ren, X. R., and Brune, W. H.: A laser-induced fluorescence instrument for detecting tropospheric OH and HO₂: Characteristics and calibration, *J. Atmos. Chem.*, 47, 139-167, 10.1023/B:JOCH.0000021036.53185.0e, 2004.
- Fleming, Z. L., Monks, P. S., Rickard, A. R., Heard, D. E., Bloss, W. J., Seakins, P. W., Still, T. J., Sommariva, R., Pilling, M. J., Morgan, R., Green, T. J., Brough, N., Mills, G. P., Penkett, S. A., Lewis, A. C., Lee, J. D., Saiz-Lopez, A., and Plane, J. M. C.: Peroxy radical chemistry and the control of ozone photochemistry at Mace Head, Ireland during the summer of 2002, *Atmos. Chem. Phys.*, 6, 2193-2214, 10.5194/acp-6-2193-2006, 2006.
- Fuchs, H., Holland, F., and Hofzumahaus, A.: Measurement of tropospheric RO₂ and HO₂ radicals by a laser-induced fluorescence instrument, *Rev. Sci. Instrum.*, 79, 084104-084112, 10.1063/1.2968712, 2008.
- Fuchs, H., Dubé, W. P., Lerner, B. M., Wagner, N. L., Williams, E. J., and Brown, S. S.: A Sensitive and Versatile Detector for Atmospheric NO₂ and NO_x Based on Blue Diode Laser Cavity Ring-Down Spectroscopy, *Environm. Sci. Technol.*, 43, 7831-7836, 10.1021/es902067h, 2009.

- 635 Furgeson, A., Mielke, L. H., Paul, D., and Osthoff, H. D.: A photochemical source of peroxypropionic and peroxyisobutanoic nitric anhydride, *Atmos. Environ.*, 45, 5025-5032, 10.1016/j.atmosenv.2011.03.072, 2011.
- Green, T. J., Reeves, C. E., Fleming, Z. L., Brough, N., Rickard, A. R., Bandy, B. J., Monks, P. S., and Penkett, S. A.: An improved dual channel PERCA instrument for atmospheric measurements of peroxy radicals, *J. Environ. Monit.*, 8, 530-536, 10.1039/B514630E 2006.
- 640 Grosjean, D., Grosjean, E., and Williams, E. L.: Thermal decomposition of PAN, PPN and vinyl-PAN, *J. Air Waste Manag. Assoc.*, 44, 391-396, 10.1080/1073161X.1994.10467260, 1994.
- Hanke, M., Uecker, J., Reiner, T., and Arnold, F.: Atmospheric peroxy radicals: ROXMAS, a new mass-spectrometric methodology for speciated measurements of HO₂ and Sigma RO₂ and first results, *Int. J. Mass Spectrom.*, 213, 91-99, 10.1016/s1387-3806(01)00548-6, 2002.
- 645 Hastie, D. R., Weissenmayer, M., Burrows, J. P., and Harris, G. W.: Calibrated chemical amplifier for atmospheric RO_x measurements, *Anal. Chem.*, 63, 2048-2057, 10.1021/ac00018a029, 1991.
- Heard, D. E.: Atmospheric field measurements of the hydroxyl radical using laser-induced fluorescence spectroscopy, *Ann. Rev. Phys. Chem.*, 57, 191-216, 10.1146/annurev.physchem.57.032905.104516, 2006.
- Heimerl, J. M., and Coffee, T. P.: The unimolecular ozone decomposition reaction, *Combustion and Flame*, 35, 650 117-123, 10.1016/0010-2180(79)90015-4, 1979.
- Hippler, H., Rahn, R., and Troe, J.: Temperature and pressure dependence of ozone formation rates in the range 1–1000 bar and 90–370 K, *The Journal of Chemical Physics*, 93, 6560-6569, 10.1063/1.458972, 1990.
- Hornbrook, R. S., Crawford, J. H., Edwards, G. D., Goyea, O., Mauldin Iii, R. L., Olson, J. S., and Cantrell, C. A.: Measurements of tropospheric HO₂ and RO₂ by oxygen dilution modulation and chemical ionization mass 655 spectrometry, *Atmos. Meas. Tech.*, 4, 735-756, 10.5194/amt-4-735-2011, 2011.

- Horstjann, M., Andres Hernandez, M. D., Nenakhov, V., Chrobry, A., and Burrows, J. P.: Peroxy radical detection for airborne atmospheric measurements using absorption spectroscopy of NO₂, *Atmos. Meas. Tech.*, 7, 1245-1257, 10.5194/amt-7-1245-2014, 2014.
- Jenkin, M. E., Saunders, S. M., and Pilling, M. J.: The tropospheric degradation of volatile organic compounds: a protocol for mechanism development, *Atmos. Environm.*, 31, 81-104, 10.1016/S1352-2310(96)00105-7, 1997.
- Jenkin, M. E., Wyche, K. P., Evans, C. J., Carr, T., Monks, P. S., Alfarra, M. R., Barley, M. H., McFiggans, G. B., Young, J. C., and Rickard, A. R.: Development and chamber evaluation of the MCM v3.2 degradation scheme for β-caryophyllene, *Atmos. Chem. Phys.*, 12, 5275-5308, 10.5194/acp-12-5275-2012, 2012.
- Jones, A. E., Brough, N., Anderson, P. S., and Wolff, E. W.: HO₂NO₂ and HNO₃ in the coastal Antarctic winter night: a "lab-in-the-field" experiment, *Atmos. Chem. Phys.*, 14, 11843-11851, 10.5194/acp-14-11843-2014, 2014.
- Jones, W. M., and Davidson, N.: The Thermal Decomposition of Ozone in a Shock Tube, *J. Am. Chem. Soc.*, 84, 2868-2878, 10.1021/ja00874a005, 1962.
- Kabir, M., Jagiella, S., and Zabel, F.: Thermal Stability of n-Acyl Peroxynitrates, *Internat. J. Chem. Kin.*, 46, 462-469, 10.1002/kin.20862, 2014.
- Kanno, N., Tonokura, K., and Koshi, M.: Equilibrium constant of the HO₂-H₂O complex formation and kinetics of HO₂+HO₂-H₂O: Implications for tropospheric chemistry, *J. Geophys. Res.-Atmos.*, 111, D20312, 10.1029/2005jd006805, 2006.
- Kim, S., Huey, L. G., Stickel, R. E., Tanner, D. J., Crawford, J. H., Olson, J. R., Chen, G., Brune, W. H., Ren, X., Leshner, R., Wooldridge, P. J., Bertram, T. H., Perring, A., Cohen, R. C., Lefer, B. L., Shetter, R. E., Avery, M., Diskin, G., and Sokolik, I.: Measurement of HO₂NO₂ in the free troposphere during the Intercontinental Chemical Transport Experiment–North America 2004, *J. Geophys. Res.-Atmos.*, 112, D12S01, 10.1029/2006jd007676, 2007.

- Kirchner, F., and Stockwell, W. R.: Effect of peroxy radical reactions on the predicted concentrations of ozone,
680 nitrogenous compounds, and radicals, *J. Geophys. Res.-Atmos.*, 101, 21007-21022, 10.1029/96jd01519, 1996.
- Kulyk, K., Zettergren, H., Gatchell, M., Alexander, J. D., Borysenko, M., Palianytsia, B., Larsson, M., and Kulik,
T.: Dimethylsilanone Generation from Pyrolysis of Polysiloxanes Filled with Nanosized Silica and Ceria/Silica,
ChemPlusChem, 81, 1003-1013, 10.1002/cplu.201600229, 2016.
- Lee, J. B., Yoon, J. S., Jung, K., Eom, S. W., Chae, Y. Z., Cho, S. J., Kim, S. D., Sohn, J. R., and Kim, K. H.:
685 Peroxyacetyl nitrate (PAN) in the urban atmosphere, *Chemosphere*, 93, 1796-1803,
10.1016/j.chemosphere.2013.06.019, 2013.
- Lee, L., Wooldridge, P. J., deGouw, J., Brown, S. S., Bates, T. S., Quinn, P. K., and Cohen, R. C.: Particulate
organic nitrates observed in an oil and natural gas production region during wintertime, *Atmos. Chem. Phys.*, 15,
9313-9325, 10.5194/acp-15-9313-2015, 2015.
- 690 Liu, Y., and Zhang, J.: Atmospheric Peroxy Radical Measurements Using Dual-Channel Chemical Amplification
Cavity Ringdown Spectroscopy, *Anal. Chem.*, 86, 5391-5398, 10.1021/ac5004689, 2014.
- Mielke, L. H., Furgeson, A., and Osthoff, H. D.: Observation of ClNO₂ in a mid-continental urban environment,
Environm. Sci. Technol., 45, 8889-8896, 10.1021/es201955u, 2011.
- Mielke, L. H., and Osthoff, H. D.: On quantitative measurements of peroxy-carboxylic nitric anhydride mixing
695 ratios by thermal dissociation chemical ionization mass spectrometry, *Int. J. Mass Spectrom.*, 310, 1-9,
10.1016/j.ijms.2011.10.005, 2012.
- Mihele, C. M., and Hastie, D. R.: The sensitivity of the radical amplifier to ambient water vapour, *Geophys. Res.
Lett.*, 25, 1911-1913, 10.1029/98gl01432, 1998.
- Mihele, C. M., Mozurkewich, M., and Hastie, D. R.: Radical loss in a chain reaction of CO and NO in the presence
700 of water: Implications for the radical amplifier and atmospheric chemistry, *Internat. J. Chem. Kin.*, 31, 145-152,
10.1002/(sici)1097-4601(1999)31:2<145::aid-kin7>3.0.co;2-m, 1999.

- Mihele, C. M., and Hastie, D. R.: Optimized operation and calibration procedures for radical amplifier-type detectors, *Journal Of Atmospheric And Oceanic Technology*, 17, 788-794, 10.1175/1520-0426(2000)017<0788:OOACPF>2.0.CO;2, 2000.
- 705 Mills, G. P., Sturges, W. T., Salmon, R. A., Bauguitte, S. J. B., Read, K. A., and Bandy, B. J.: Seasonal variation of peroxyacetyl nitrate (PAN) in coastal Antarctica measured with a new instrument for the detection of sub-part per trillion mixing ratios of PAN, *Atmos. Chem. Phys.*, 7, 4589-4599, 10.5194/acp-7-4589-2007, 2007.
- Murphy, J. G., Thornton, J. A., Wooldridge, P. J., Day, D. A., Rosen, R. S., Cantrell, C., Shetter, R. E., Lefer, B., and Cohen, R. C.: Measurements of the sum of HO₂NO₂ and CH₃O₂NO₂ in the remote troposphere, *Atmos. Chem.*
710 *Phys.*, 4, 377-384, 10.5194/acp-4-377-2004, 2004.
- Odame-Ankrah, C. A., and Osthoff, H. D.: A compact diode laser cavity ring-down spectrometer for atmospheric measurements of NO₃ and N₂O₅ with automated zeroing and calibration, *Appl. Spectrosc.*, 65, 1260-1268, 10.1366/11-06384, 2011.
- Odame-Ankrah, C. A.: Improved detection instrument for nitrogen oxide species, Ph.D., Chemistry, University of
715 Calgary, <http://hdl.handle.net/11023/2006>, 10.5072/PRISM/26475, Calgary, 2015.
- Paul, D., Furgeson, A., and Osthoff, H. D.: Measurements of total peroxy and alkyl nitrate abundances in laboratory-generated gas samples by thermal dissociation cavity ring-down spectroscopy, *Rev. Sci. Instrum.*, 80, 114101, 10.1063/1.3258204 2009.
- Paul, D., and Osthoff, H. D.: Absolute Measurements of Total Peroxy Nitrate Mixing Ratios by Thermal
720 Dissociation Blue Diode Laser Cavity Ring-Down Spectroscopy, *Anal. Chem.*, 82, 6695-6703, 10.1021/ac101441z, 2010.
- Perez, I. M., Wooldridge, P. J., and Cohen, R. C.: Laboratory evaluation of a novel thermal dissociation chemiluminescence method for in situ detection of nitrous acid, *Atmos. Environm.*, 41, 3993-4001, 10.1016/j.atmosenv.2007.01.060, 2007.

- 725 Phillips, G. J., Pouvesle, N., Thieser, J., Schuster, G., Axinte, R., Fischer, H., Williams, J., Lelieveld, J., and
Crowley, J. N.: Peroxyacetyl nitrate (PAN) and peroxyacetic acid (PAA) measurements by iodide chemical
ionisation mass spectrometry: first analysis of results in the boreal forest and implications for the measurement
of PAN fluxes, *Atmos. Chem. Phys.*, 13, 1129-1139, 10.5194/acp-13-1129-2013, 2013.
- Portmann, R. W., Brown, S. S., Gierczak, T., Talukdar, R. K., Burkholder, J. B., and Ravishankara, A. R.: Role of
730 nitrogen oxides in the stratosphere: A reevaluation based on laboratory studies, *Geophys. Res. Lett.*, 26, 2387-
2390, 10.1029/1999GL900499, 1999.
- Roberts, J. M.: The atmospheric chemistry of organic nitrates, *Atmos. Environ. A*, 24, 243-287, 10.1016/0960-
1686(90)90108-Y, 1990.
- Roberts, J. M.: PAN and Related Compounds, in: *Volatile Organic Compounds in the Atmosphere*, edited by:
735 Koppmann, R., Blackwell Publishing, Oxford, UK, 221-268, 2007.
- Rollins, A. W., Smith, J. D., Wilson, K. R., and Cohen, R. C.: Real Time In Situ Detection of Organic Nitrates in
Atmospheric Aerosols, *Environm. Sci. Technol.*, 44, 5540-5545, 10.1021/es100926x, 2010.
- Rücker, C., and Kümmerer, K.: Environmental Chemistry of Organosiloxanes, *Chem. Rev.*, 115, 466-524,
10.1021/cr500319v, 2015.
- 740 Sadanaga, Y., Takaji, R., Ishiyama, A., Nakajima, K., Matsuki, A., and Bandow, H.: Thermal dissociation cavity
attenuated phase shift spectroscopy for continuous measurement of total peroxy and organic nitrates in the clean
atmosphere, *Rev. Sci. Instrum.*, 87, 074102, 10.1063/1.4958167, 2016.
- Sahetchian, K. A., Rigny, R., Tardieu de Maleissye, J., Batt, L., Anwar Khan, M., and Mathews, S.: The pyrolysis
of organic hydroperoxides (ROOH), *Symposium (International) on Combustion*, 24, 637-643, 10.1016/S0082-
745 0784(06)80078-0, 1992.
- Sandu, A., and Sander, R.: Technical note: Simulating chemical systems in Fortran90 and Matlab with the Kinetic
PreProcessor KPP-2.1, *Atmos. Chem. Phys.*, 6, 187-195, 10.5194/acp-6-187-2006, 2006.

- Saunders, S. M., Jenkin, M. E., Derwent, R. G., and Pilling, M. J.: Protocol for the development of the Master Chemical Mechanism, MCM v3 (Part A): tropospheric degradation of non-aromatic volatile organic compounds, 750 *Atmos. Chem. Phys.*, 3, 161-180, 10.5194/acp-3-161-2003, 2003.
- Schmidt, C., and Sehon, A. H.: The thermal decomposition of peracetic acid in the vapor phase, *Canadian Journal of Chemistry*, 41, 1819-1825, 10.1139/v63-261, 1963.
- Singh, H. B., Herlth, D., Ohara, D., Zahnle, K., Bradshaw, J. D., Sandholm, S. T., Talbot, R., Crutzen, P. J., and Kanakidou, M.: Relationship of peroxyacetyl nitrate to active and total odd nitrogen at northern high-latitudes - 755 influence of reservoir species on NO_x and O₃, *J. Geophys. Res.-Atmos.*, 97, 16523-16530, 10.1029/91jd00890, 1992.
- Singh, H. B., Brune, W. H., Crawford, J. H., Jacob, D. J., and Russell, P. B.: Overview of the summer 2004 Intercontinental Chemical Transport Experiment–North America (INTEX-A), *J. Geophys. Res.-Atmos.*, 111, D24S01, 10.1029/2006jd007905, 2006.
- 760 Slusher, D. L., Pitteri, S. J., Haman, B. J., Tanner, D. J., and Huey, L. G.: A chemical ionization technique for measurement of pernitric acid in the upper troposphere and the polar boundary layer, *Geophysical Research Letters*, 28, 3875-3878, 10.1029/2001gl013443, 2001.
- Slusher, D. L., Huey, L. G., Tanner, D. J., Flocke, F. M., and Roberts, J. M.: A thermal dissociation-chemical ionization mass spectrometry (TD-CIMS) technique for the simultaneous measurement of peroxyacyl nitrates and 765 dinitrogen pentoxide, *J. Geophys. Res.*, 109, D19315, 10.1029/2004JD004670, 2004.
- Sobanski, N., Schuladen, J., Schuster, G., Lelieveld, J., and Crowley, J. N.: A five-channel cavity ring-down spectrometer for the detection of NO₂, NO₃, N₂O₅, total peroxy nitrates and total alkyl nitrates, *Atmos. Meas. Tech.*, 9, 5103-5118, 10.5194/amt-9-5103-2016, 2016.
- Solomon, S.: Stratospheric ozone depletion: A review of concepts and history, *Rev. Geophys.*, 37, 275-316, 770 10.1029/1999RG900008, 1999.

- Spencer, K. M., McCabe, D. C., Crouse, J. D., Olson, J. R., Crawford, J. H., Weinheimer, A. J., Knapp, D. J., Montzka, D. D., Cantrell, C. A., Hornbrook, R. S., Mauldin, R. L., and Wennberg, P. O.: Inferring ozone production in an urban atmosphere using measurements of peroxyacetic acid, *Atmos. Chem. Phys.*, 9, 3697-3707, 10.5194/acp-9-3697-2009, 2009.
- 775 Stenke, A., and Grewe, V.: Simulation of stratospheric water vapor trends: impact on stratospheric ozone chemistry, *Atmos. Chem. Phys.*, 5, 1257-1272, 10.5194/acp-5-1257-2005, 2005.
- Taha, Y. M., Saowapon, M. T., and Osthoff, H. D.: Detection of triacetone triperoxide by thermal decomposition peroxy radical chemical amplification coupled to cavity ring-down spectroscopy, *Anal. Bioanal. Chem.*, 410, 4203-4212, 10.1007/s00216-018-1072-0, 2018.
- 780 Thaler, R. D., Mielke, L. H., and Osthoff, H. D.: Quantification of Nitryl Chloride at Part Per Trillion Mixing Ratios by Thermal Dissociation Cavity Ring-Down Spectroscopy, *Anal. Chem.*, 83, 2761-2766, 10.1021/ac200055z, 2011.
- Thieser, J., Schuster, G., Schuladen, J., Phillips, G. J., Reiffs, A., Parchatka, U., Pöhler, D., Lelieveld, J., and Crowley, J. N.: A two-channel thermal dissociation cavity ring-down spectrometer for the detection of ambient
785 NO_2 , RO_2NO_2 and RONO_2 , *Atmos. Meas. Tech.*, 9, 553-576, 10.5194/amt-9-553-2016, 2016.
- Tokarek, T. W., Huo, J. A., Odame-Ankrah, C. A., Hammoud, D., Taha, Y. M., and Osthoff, H. D.: A gas chromatograph for quantification of peroxyacetic nitric anhydrides calibrated by thermal dissociation cavity ring-down spectroscopy, *Atmos. Meas. Tech.*, 7, 3263-3283, 10.5194/amt-7-3263-2014, 2014.
- Tuazon, E. C., Winer, A. M., and Pitts, J. N.: Trace pollutant concentrations in a multiday smog episode in the
790 California South Coast Air Basin by long path length Fourier transform infrared spectroscopy, *Environm. Sci. Technol.*, 15, 1232-1237, 10.1021/es00092a014, 1981.
- Veres, P. R., Roberts, J. M., Wild, R. J., Edwards, P. M., Brown, S. S., Bates, T. S., Quinn, P. K., Johnson, J. E., Zamora, R. J., and de Gouw, J.: Peroxyacetic acid (HO_2NO_2) measurements during the UBWOS 2013 and 2014

- studies using iodide ion chemical ionization mass spectrometry, *Atmos. Chem. Phys.*, 15, 8101-8114, 795 10.5194/acp-15-8101-2015, 2015.
- Wild, R. J., Edwards, P. M., Dube, W. P., Baumann, K., Edgerton, E. S., Quinn, P. K., Roberts, J. M., Rollins, A. W., Veres, P. R., Warneke, C., Williams, E. J., Yuan, B., and Brown, S. S.: A Measurement of Total Reactive Nitrogen, NO_y , together with NO_2 , NO , and O_3 via Cavity Ring-down Spectroscopy, *Environm. Sci. Technol.*, 48, 9609-9615, 10.1021/es501896w, 2014.
- 800 Womack, C. C., Neuman, J. A., Veres, P. R., Eilerman, S. J., Brock, C. A., Decker, Z. C. J., Zarzana, K. J., Dube, W. P., Wild, R. J., Wooldridge, P. J., Cohen, R. C., and Brown, S. S.: Evaluation of the accuracy of thermal dissociation CRDS and LIF techniques for atmospheric measurement of reactive nitrogen species, *Atmos. Meas. Tech. Discuss.*, 2016, 1-30, 10.5194/amt-2016-398, 2016.
- Womack, C. C., Neuman, J. A., Veres, P. R., Eilerman, S. J., Brock, C. A., Decker, Z. C. J., Zarzana, K. J., Dube, 805 W. P., Wild, R. J., Wooldridge, P. J., Cohen, R. C., and Brown, S. S.: Evaluation of the accuracy of thermal dissociation CRDS and LIF techniques for atmospheric measurement of reactive nitrogen species, *Atmos. Meas. Tech.*, 10, 1911-1926, 10.5194/amt-10-1911-2017, 2017.
- Wood, E. C., Deming, B. L., and Kundu, S.: Ethane-Based Chemical Amplification Measurement Technique for Atmospheric Peroxy Radicals, *Environmental Science & Technology Letters*, 4, 15-19, 810 10.1021/acs.estlett.6b00438, 2016.
- Wooldridge, P. J., Perring, A. E., Bertram, T. H., Flocke, F. M., Roberts, J. M., Singh, H. B., Huey, L. G., Thornton, J. A., Wolfe, G. M., Murphy, J. G., Fry, J. L., Rollins, A. W., LaFranchi, B. W., and Cohen, R. C.: Total Peroxy Nitrates (ΣPNs) in the atmosphere: the Thermal Dissociation-Laser Induced Fluorescence (TD-LIF) technique and comparisons to speciated PAN measurements, *Atmos. Meas. Tech.*, 3, 593-607, 10.5194/amt-3-593-2010, 815 2010.

Zheng, W., Flocke, F. M., Tyndall, G. S., Swanson, A., Orlando, J. J., Roberts, J. M., Huey, L. G., and Tanner, D.

J.: Characterization of a thermal decomposition chemical ionization mass spectrometer for the measurement of peroxy acyl nitrates (PANs) in the atmosphere, *Atmos. Chem. Phys.*, 11, 6529-6547, 10.5194/acp-11-6529-2011, 2011.

820 Ziemann, P. J., and Atkinson, R.: Kinetics, products, and mechanisms of secondary organic aerosol formation, *Chem. Soc. Rev.*, 41, 6582-6605, 10.1039/c2cs35122f, 2012.

Table 1. Typical* PNA and PAN mixing ratios in various environments where both were quantified.

Location	PNA (pptv)	PAN (pptv)	PNA/PAN
Antarctica - Summer	20 (Slusher et al., 2001)	15.6 (Eisele et al., 2008)	1.3
Antarctica - Summer	22 (Jones et al., 2014)	15.6 (Eisele et al., 2008)	1.4
Antarctica – Summer	2.5 (Jones et al., 2014)	9.2 (Mills et al., 2007)	0.27
Remote troposphere – Spring	-	-	0.13** (Murphy et al., 2004)
Free troposphere (Intex-NA) - Summer	45 (Kim et al., 2007)	280 (Singh et al., 2006)	0.16***
Uintah Basin – Winter 2013	500 (Veres et al., 2015)	2000 (Ahmadov et al., 2015)	0.25
Uintah Basin – Winter 2014	100 (Veres et al., 2015)	300 (Lee et al., 2015)	0.33
Atlanta – Winter	3.7 (Chen et al., 2017a)	640-800 (Lee et al., 2013)	<0.01
Atlanta – Summer	11.7 (Chen et al., 2017a)	640-800 (Lee et al., 2013)	0.01-0.02

* Average values

** calculated assuming all non-PAN and PPN peroxy nitrate is PNA.

830 *** Averages of data posted on ftp://ftp-air.larc.nasa.gov/pub/INTEXA/DC8_AIRCRAFT/

Table 2. Selected thermal dissociation methods for quantification of daytime NO_v species.

<u>Species quantified</u>	<u>NO₂ detection method</u>	<u>Group</u>	<u>Reference</u>
<u>NO₂, ΣPAN, ΣAN, HNO₃</u>	<u>LIF</u>	<u>Berkeley</u>	(Day et al., 2002)
<u>ΣPN</u>	<u>LIF</u>	<u>Berkeley</u>	(Murphy et al., 2004)
<u>HONO</u>	<u>CL</u>	<u>Berkeley</u>	<u>(Perez et al., 2007)</u>
<u>NO₂, ΣPAN, ΣAN</u>	<u>CRDS</u>	<u>Calgary</u>	(Paul et al., 2009)
<u>Aerosol nitrates</u>	<u>LIF</u>	<u>Berkeley</u>	(Rollins et al., 2010)
<u>CINO₂</u>	<u>CRDS</u>	<u>Calgary</u>	(Thaler et al., 2011)
<u>NO₂, ΣPAN, ΣAN, HNO₃</u>	<u>LIF</u>	<u>L'Aquila</u>	<u>(Di Carlo et al., 2013)</u>
<u>NO, NO₂, HONO, NO_y, ammonium nitrate</u>	<u>CRDS</u>	<u>NOAA</u>	(Wild et al., 2014; Womack et al., 2017)
<u>NO₂, ΣPAN, ΣAN</u>	<u>CRDS</u>	<u>Max-Planck-Institut</u>	(Thieser et al., 2016)
<u>NO₂, ΣPAN, ΣAN</u>	<u>CAPS</u>	<u>Osaka</u>	<u>(Sadanaga et al., 2016)</u>
<u>NO₂, RNO₂</u>	<u>CRDS</u>	<u>Hefei</u>	(Chen et al., 2017b)
<u>ΣPN, ΣPAN</u>	<u>PERCA-CRDS</u>	<u>Calgary</u>	<u>this work</u>

Table 2/ Table 3. List of chemical reactions*

Number	Reaction	k (cm ³ molecule ⁻¹ s ⁻¹)	k _{298K} (cm ³ molecule ⁻¹ s ⁻¹)
R1	CH ₃ O ₂ + NO → CH ₃ O + NO ₂	2.3×10 ⁻¹² × e ^(360/T)	7.7×10 ⁻¹²
R2	CH ₃ O + O ₂ → HCHO + HO ₂	7.2×10 ⁻¹⁴ × e ^(-1080/T)	1.9×10 ⁻¹⁵
R3	HO ₂ + NO → HO + NO ₂	3.5×10 ⁻¹² × e ^(270/T)	8.5×10 ⁻¹²
R4	C ₂ H ₆ + HO + O ₂ → H ₂ O + C ₂ H ₅ O ₂	6.9×10 ⁻¹² × e ^(-1000/T)	2.4×10 ⁻¹³
R5	C ₂ H ₅ O ₂ + NO → C ₂ H ₅ O + NO ₂	2.55×10 ⁻¹² × e ^(380/T) × 0.99	9.1×10 ⁻¹²
R6	C ₂ H ₅ O + O ₂ → CH ₃ CHO + HO ₂	2.4×10 ⁻¹⁴ × e ^(-325/T)	8.1×10 ⁻¹⁵
R7	PAN → CH ₃ CO ₃ + NO ₂	See Table 3/ Table 4	4.4×10 ⁻⁴ s ⁻¹
R8	CH ₃ C(O)O ₂ + NO → NO ₂ + CH ₃ C(O)O → NO ₂ + CH ₃ + CO ₂	7.5×10 ⁻¹² × e ^(290/T)	2.0×10 ⁻¹¹
R9	PPN → C ₂ H ₅ CO ₃ + NO ₂	See Table 34	3.7×10 ⁻⁴ s ⁻¹
R10	C ₂ H ₅ CO ₃ +NO+O ₂ → C ₂ H ₅ O ₂ +NO ₂ +CO ₂	6.7×10 ⁻¹² × e ^(340/T)	2.1×10 ⁻¹¹
R11	HO + NO + M → HONO + M	7.4×10 ⁻³¹ × (T/300) ^{-2.4} × [M]	9.7×10 ⁻¹² **
R12	HO ₂ + NO ₂ + M → HO ₂ NO ₂ + M	(termolecular)	(termolecular)
R13	HO ₂ + HO ₂ + M → H ₂ O ₂ + M	(termolecular)	(termolecular)
R14	CH ₃ CO ₃ → 0.7 CH ₃ CO ₂ + 0.3 CH ₃ CO ₂ H	5.0×10 ⁻¹² × ∑RO ₂	5.0×10 ⁻¹² × ∑RO ₂
R15	C ₂ H ₅ CO ₃ → 0.7 C ₂ H ₅ CO ₂ + 0.3 C ₂ H ₅ CO ₂ H	5.0×10 ⁻¹² × ∑RO ₂	5.0×10 ⁻¹² × ∑RO ₂
R16	CH ₃ O ₂ → 0.330 CH ₃ O + 0.335 HCHO + 0.335 CH ₃ OH	1.8×10 ⁻¹³ × e ^(416/T) × ∑RO ₂	7.4×10 ⁻¹³ × ∑RO ₂
R17	C ₂ H ₅ O ₂ → 0.6 C ₂ H ₅ O + 0.2 CH ₃ CHO + 0.2 C ₂ H ₅ OH	3.1×10 ⁻¹³ × ∑RO ₂	3.1×10 ⁻¹³ × ∑RO ₂

835 * Rate constant expressions are from the Master Chemical Mechanism (MCM), (Jenkin et al., 1997; Saunders et al., 2003) version 3.3.1, except R7 and R9, which are from Kabir et al. (2014)

** calculated using [O₂] = 4.2×10¹⁸ molecules cm⁻³

840 **Table 3** **Table 4:** Arrhenius parameters for thermal dissociation of selected PN, PAN, PPN, PAA, and O₃.

Molecule	A (s ⁻¹)	E _a (kJ mol ⁻¹)	Reference	T needed to dissociate 0.1% (°C)**	T needed to dissociate 99.9% (°C)**
HO ₂ NO ₂ (PNA)	7.3×10 ¹⁴ *	88.1±4.4	(Atkinson et al., 1997)	24	123
CH ₃ O ₂ NO ₂ (MPN)	1.1×10 ¹⁶	88.1±4.4	(Atkinson et al., 1997)	3	86
C ₂ H ₅ O ₂ NO ₂ (EPN)	8.8×10 ¹⁵	86.5±8.7	(Atkinson et al., 1997)	0	82
CH ₃ C(O)O ₂ NO ₂ (PAN)	2.8×10 ¹⁶	113±2	(Kabir et al., 2014)	73	174
C ₂ H ₅ C(O)O ₂ NO ₂ (PPN)	2.36×10 ¹⁶	113±2	(Kabir et al., 2014)	75	176
CH ₃ C(O)O ₂ H (PAA)	10 ¹⁴	134±8	(Schmidt and Sehon, 1963)	206	377
CH ₃ C(O)O ₂ H (PAA)	1.15×10 ¹³	136	(Devush et al., 1983)	247	450
CH ₃ C(O)O ₂ H (PAA)	5×10 ¹⁴	168±4	(Sahetchian et al., 1992)	300	492
O ₃	1.3×10 ¹⁰ *	92.8	(Jones and Davidson, 1962; Heimerl and Coffee, 1979)	180	433

* Calculated assuming a pressure of 550 Torr and temperature of 298 K.

** Assuming a contact time of 4 ms at the maximum temperature (Paul et al., 2009)

Table 4 Table 5: Products of CL and F for PNA and PAN at 110 °C, 80 °C, and 60 °C (RH = 34%)

	CL _{110 °C} × F _{110 °C}	CL _{80 °C} × F _{80 °C}	CL _{60 °C} × F _{60 °C}
PNA	41.8 ± 0.2	39.5 ± 0.2	31.9 ± 0.1
ΣPAN	10 ± 1	7.6 ± 0.9	1.2 ± 0.2

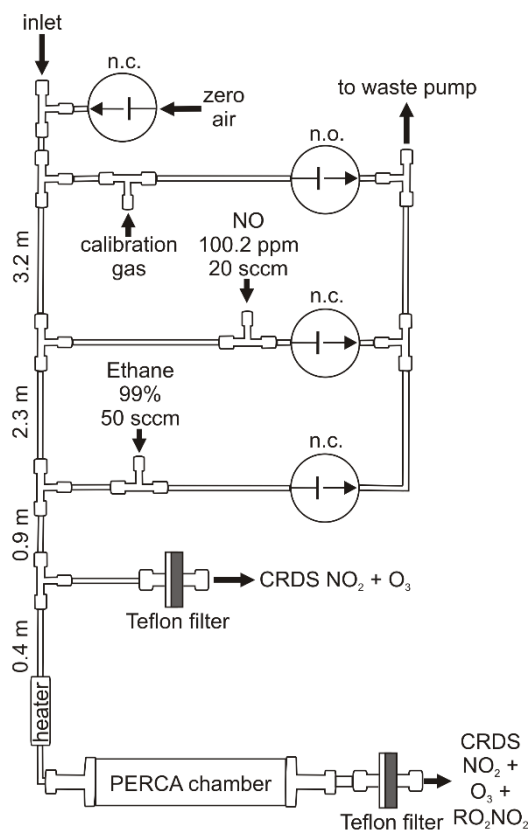
850 **Table 5 Table 6: Statistics (average ± 1 standard deviation) of the 1 s data shown in Figure 12.**

Time period	PNA (pptv)			PAN (pptv)		
	T1 = 110 °C T2 = 60 °C	T1 = 110 °C T2 = 80 °C	T1 = 80 °C T2 = 60 °C	T1 = 110 °C T2 = 60 °C	T1 = 110 °C T2 = 80 °C	T1 = 80 °C T2 = 60 °C
21:48:45 – 21:49:15	266 ± 4	254 ± 17	267 ± 4	447 ± 26	495 ± 75	430 ± 31
21:51:15 – 21:52:45	261 ± 5	258 ± 14	261 ± 6	480 ± 32	491 ± 68	476 ± 38

Table 67: Statistics (average \pm 1 standard deviation) of the 1 s data of laboratory air (first time period), laboratory air spiked with ~260 pptv PNA (second period), and laboratory air spiked with 260 pptv PNA and ~480 pptv PAN (third period). n/a = not applicable.

Time period	Σ PN (ppbv)			Σ PAN (ppbv)		
	T1 = 110 °C T2 = 60 °C	T1 = 110 °C T2 = 80 °C	T1 = 80 °C T2 = 60 °C	T1 = 110 °C T2 = 60 °C	T1 = 110 °C T2 = 80 °C	T1 = 80 °C T2 = 60 °C
Room air	-0.08 \pm 0.01	-0.29 \pm 0.03	-0.068 \pm 0.004	4.21 \pm 0.04	5.1 \pm 0.1	3.89 \pm 0.03
Room air + PNA	0.19 \pm 0.01	-0.03 \pm 0.02	0.20 \pm 0.01	3.50 \pm 0.03	4.4 \pm 0.1	3.17 \pm 0.04
$\Delta(\Sigma$ PN)	0.27 \pm 0.01	0.26 \pm 0.04	0.27 \pm 0.01	n/a	n/a	n/a
Room air + PNA + PAN	0.19 \pm 0.01	-0.02 \pm 0.02	0.20 \pm 0.01	3.99 \pm 0.04	4.8 \pm 0.1	3.70 \pm 0.03
$\Delta(\Sigma$ PAN)	n/a	n/a	n/a	0.49 \pm 0.04	0.40 \pm 0.14	0.52 \pm 0.05

Figures



860 **Figure 1. Schematic of the dual-channel thermal decomposition peroxy radical chemical amplification inlet.**
The inlet consists of a 60 cm long, 0.635 cm (1/4") o.d. quartz heater and an 80 cm long, 1.27 cm (1/2") o.d.
FEP Teflon™ reaction chamber. Reaction gases were added upstream of the PERCA chamber by closing
the normally open valves connected to a waste pump via 50 μm critical orifices. Background NO₂ levels were
monitored in a parallel detection channel by tapping into the inlet prior to thermal dissociation of peroxy
 865 **nitrates.**

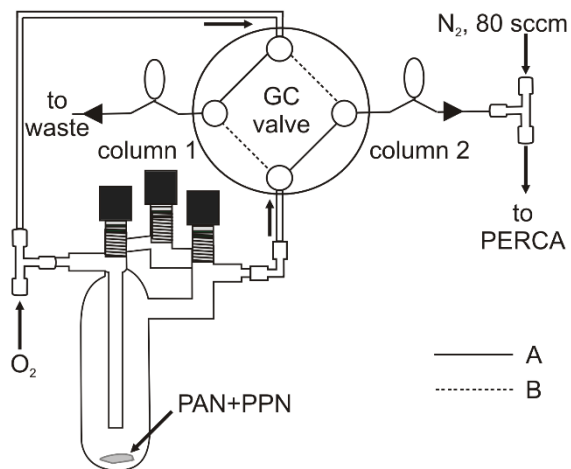


Figure 2. Setup for delivery of PAN and PPN using a gas chromatography column.

870

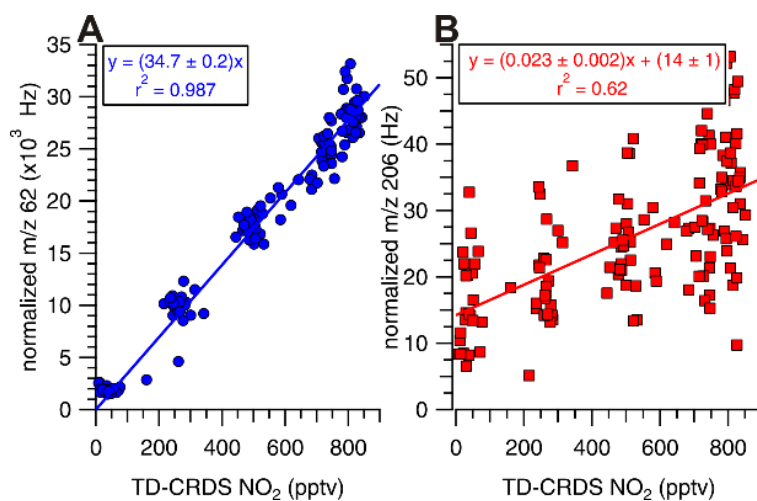


Figure 3. Calibration of CIMS response factors against TD-CRDS operated with its inlet heated to 120 °C and without amplification. (A) m/z 62. (B) m/z 206. CIMS counts were normalized to 10^6 I⁻ counts.

875

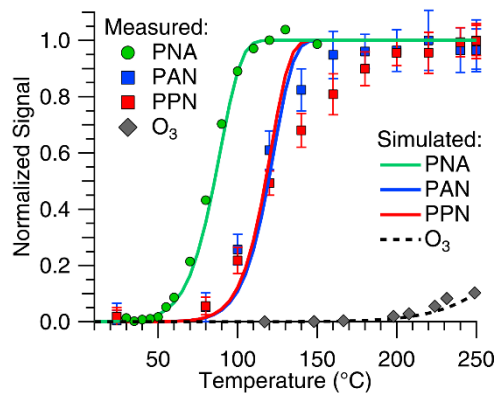


Figure 4. Normalized thermal dissociation profiles of PNA, PAN, PPN, and O₃ as a function of inlet set temperature. Superimposed trend lines are simulations based on the TD model introduced by Paul et al. (2009). The PNA, PAN, and PPN data were observed by TD-CRDS without amplification gases present, whereas the O₃ data were observed by TD-PERCA-CRDS. The error bars represent standard deviations of 1 s data.

880

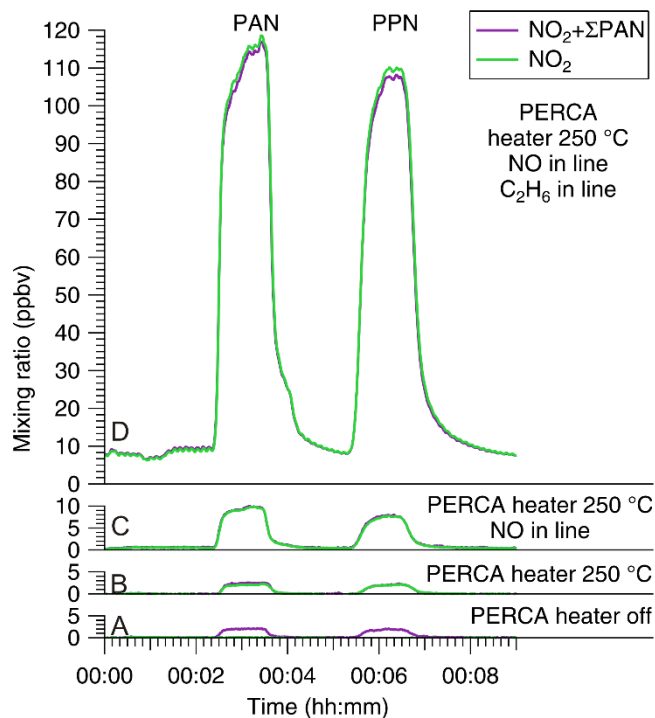


Figure 5. Peroxy radical chemical amplification of peroxyacetic and peroxypropionic nitric anhydride (PAN and PPN) delivered via a megabore GC column. (A) Time series of the signal observed by cavity ring-down spectroscopy in the ambient temperature (NO_2 ; green colour) and heated ($\text{NO}_2 + \Sigma\text{PAN}$; purple colour) channels with the PERCA heater off. (B) Same as (A) with the PERCA heater switched on. (C) Same as (B) with 0.75 ppmv NO added. (D) Same as (C) with 1.5% C_2H_6 added. The amplification factor is determined from the ratio of the ambient temperature (i.e., NO_2) CRDS signal observed in (D) divided by that observed in (B).

890

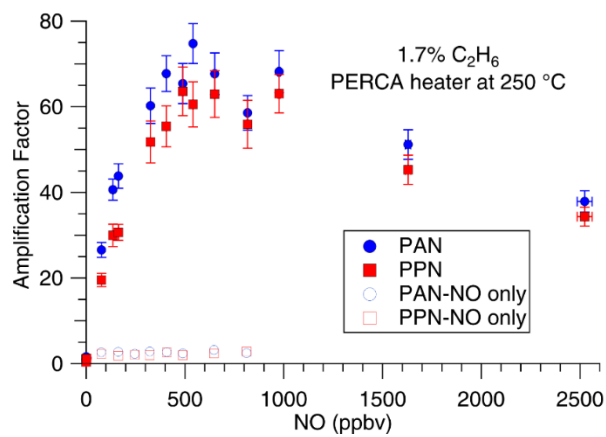


Figure 6. TD-PERCA-CRDS amplification factors of ~0.5 ppbv PAN and ~1.3 ppbv PPN as a function of NO mixing ratio at RH = 0%. The error bars represent standard deviations of 1 s data.

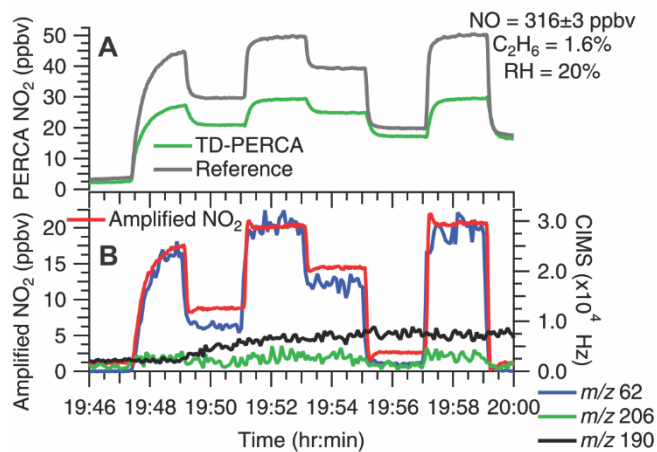


Figure 7. (A) Sample time series of PNA observed by TD-PERCA-CRDS in the reference, NO₂ channel (shown in green) and PERCA channel (grey). (B) (left) Difference signal between amplified and reference channel (shown in red). (right) CIMS counts (normalized to 10⁶ I⁻) at *m/z* 62, the major fragment (NO₃⁻) expected from PNA, at *m/z* 206 (multiplied by a factor of 100 for clarity), the HNO₄·I⁻ cluster, and at *m/z* 190, the HNO₃·I⁻ cluster.

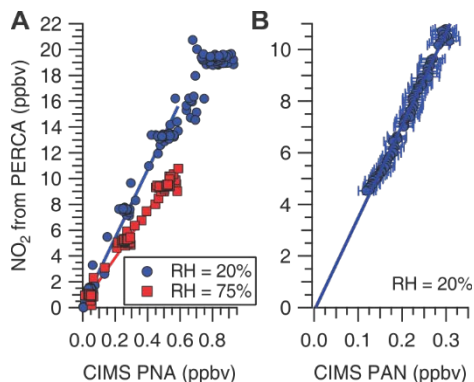
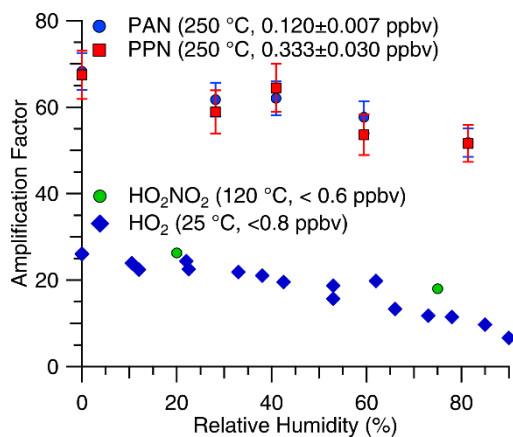


Figure 8. Scatter plots of TD-PERCA-CRDS and CIMS measurements. (A) Sample PNA calibrations at an NO mixing ratio of 316 ± 3 ppbv and TD-PERCA inlet temperature of $120\text{ }^{\circ}\text{C}$. For mixing ratios < 0.6 ppbv, the intercept and slope of the linear fits are (0.2 ± 0.1) ppbv and 26.3 ± 0.4 ($r^2 = 0.979$) at RH = 20% and (0.3 ± 0.1) ppbv and 18.0 ± 0.2 ($r^2 = 0.985$) at RH = 75%. (B) Sample PAN calibration at an NO mixing ratio of 662 ± 2 ppbv and TD-PERCA inlet temperature of $250\text{ }^{\circ}\text{C}$ and RH = 20%. The intercept and slope of the linear fit is (-0.13 ± 0.09) ppbv and 36.0 ± 0.4 ($r^2 = 0.990$).



920 **Figure 9. TD-PERCA-CRDS amplification factor as a function of relative humidity at an ethane mixing ratio of 1.6% and with NO mixing ratios of 644 ± 2 and 316 ± 3 ppbv for the PAN/PPN experiments and the PNA experiments, respectively. The PAN and PPN mixing ratios were 0.120 ± 0.007 and 0.333 ± 0.030 ppbv, respectively. The PNA mixing ratio was varied between 0 and 0.6 ppbv. The room temperature HO₂ data are from Wood et al. (2016).**

925

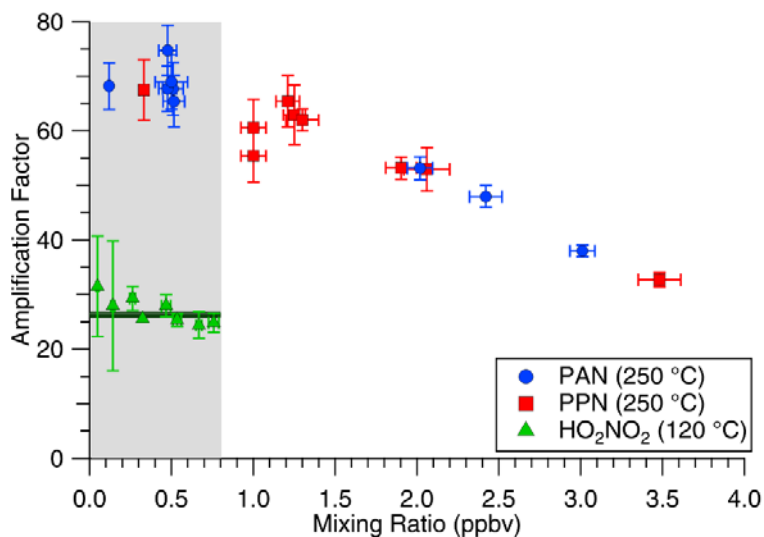
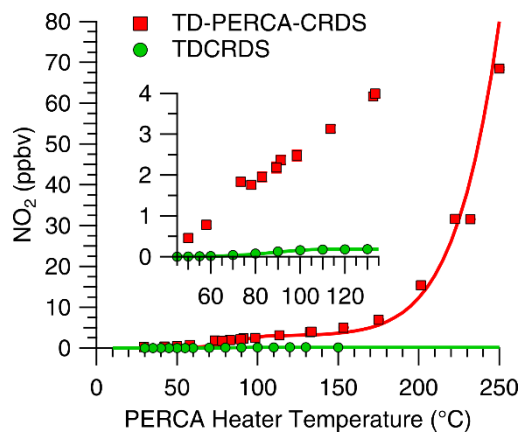
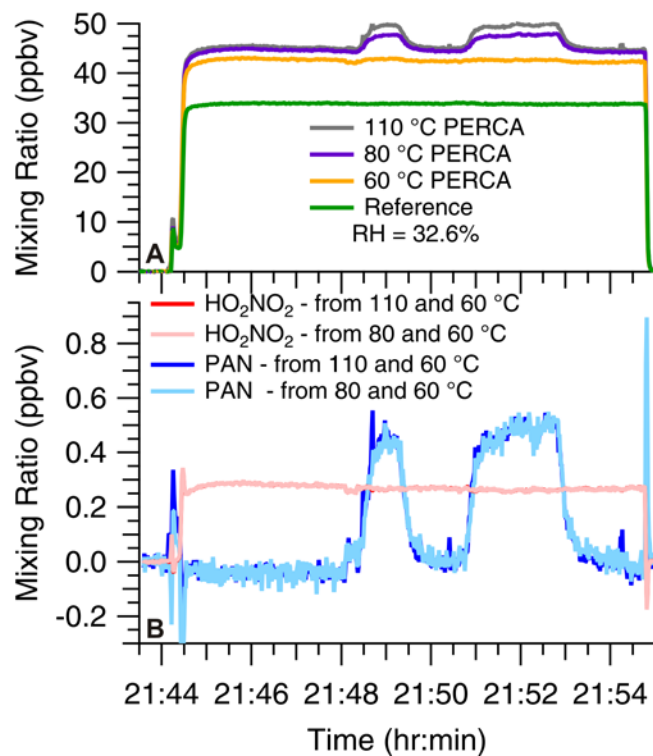


Figure 10. TD-PERCA-CRDS amplification factors as a function of PAN, PPN, and PNA mixing ratio. Errors bars correspond to $\pm 1\sigma$ standard deviation. Mixing ratios of NO and ethane were 500 ± 50 ppbv and $\sim 1.6\%$, respectively. The grey underlay indicates the linear range. The dark green line corresponds to 930 26.3 ± 0.4 (slope of data shown in Figure 8A).



935 **Figure 11. Amplification of photochemically generated PNA (red) as a function of PERCA heater temperature (RH=24%). Simultaneous quantification by CIMS and UV absorption showed that the gas stream contained 180 ± 28 pptv PNA and 3.5 ± 0.2 ppbv O₃. The non-amplified TD-CRDS signal (from Figure 4), multiplied by 0.18, is shown in green for comparison.**

940



945 **Figure 12. Demonstration of differential temperature TD-PERCA-CRDS. (A) Time series of NO₂ mixing ratios observed by an unheated reference channel and three TD-PERCA channels operated at 60 °C, 80 °C, and 110 °C, respectively. PNA was sampled from 21:44:30 to 21:54:45, and PAN was added at ~21:49 and ~21:52. (B) Mixing ratios of PAN and PNA calculated from (A).**

Supplemental Information for:

Quantification of peroxyxynitric acid and peroxyacyl nitrates using an ethane-based thermal dissociation peroxy radical chemical amplification cavity ring-down spectrometer

Youssef M. Taha¹, Matthew T. Saowapon¹, Faisal V. Assad¹, Connie Z. Ye¹, Xining Chen^{1,a},
Natasha M. Garner¹, and Hans D. Osthoff¹

¹Department of Chemistry, University of Calgary, 2500 University Drive N.W., Calgary, Alberta, Canada T2N 1N4

^a now at: Department of Chemistry, McGill University, 801 Sherbrooke St. West, Montreal, Quebec, Canada H3A

2K6

Correspondence to: Hans D. Osthoff (hosthoff@ucalgary.ca)

Table of Contents

Table of Contents	2
S1.0 Box simulations of ethane PERCA chemistry	3
S1.1 MCM only simulations	3
Table S1. Model inputs for simulations run at 25 °C and 250 °C	4
Figure S1. Time series of peroxy radicals (left-hand axis) and hydroxyl radicals (right-hand axis) for a simulation initiated with 15 pptv of HO ₂ at 25 °C.	4
Figure S2. Time series of peroxy radicals (left-hand axis) and hydroxyl radicals for a simulation initiated with 15 pptv of HO ₂ at 250 °C.....	5
Figure S3. Time series of CL for simulations initiated with 100, 300, 600, 900, and 1200 pptv of CH ₃ O ₂ at 25 °C (blue colors) and 250 °C (red colors).	6
S1.2 Inclusion of HO ₂ .H ₂ O cluster in the mechanism	6
Figure S4. Time series of CL for simulations at different RH and initiated with 15 pptv of HO ₂ at 25 °C (blue colors) and 250 °C (red colors).	7
Figure S5. Time series of CL for simulations at 20% RH initiated with different HO ₂ mixing ratios at 25 °C (blue colors) and 250 °C (red colors).	7
S1.3 Inclusion of wall losses in the mechanism.....	8
Figure S6. Time series of CL for simulations at 20% RH initiated as a function of HO ₂ mixing ratios at 25 °C (blue colors) and 250 °C (red colors) with $k_{\text{wall}}(\text{HO}_2)$ and $k_{\text{wall}}(\text{RO}_2)$ of 2.8 s ⁻¹ and 0.8 s ⁻¹ , respectively.	8
S1.4 Inclusion of ethyl nitrite formation in the mechanism.....	9
Figure S7. Same as Figure S6 but with C ₂ H ₅ ONO formation and thermal decomposition included in the mechanism.	10

S1.0 Box simulations of ethane PERCA chemistry

Box model simulations were carried out using a subset of reactions in the "Master Chemical Mechanism" (MCM) (Jenkin et al., 1997; Saunders et al., 2003; Jenkin et al., 2012) to aid in the interpretation of experimental data and are not intended as accurate representations of experiments. To reproduce the experimental data in PERCA reaction chambers, models need to make assumptions about the magnitudes and temperature dependencies of wall loss rates (which are not known). An additional limitation is that the MCM has only been validated at ambient temperature and below, and the rate constants are more uncertain at elevated temperatures. In addition, thermal gradients within the PERCA chambers are not taken into account. Thus, simulations are poor a priori predictors of experimental chain lengths and should not be viewed as such.

In section S1.1 below, we carried out simulations using only a subset of reactions in the MCM to probe the temperature dependence of gas-phase reactions. In section S1.2, we added pseudo first-order loss rates for OH and RO₂ radicals to simulate the potential effects of inner walls of the PERCA reactor. In section S1.3, we investigated the humidity dependence of PERCA, adding HO₂·H₂O chemistry using the equilibrium constants by Kanno et al. (2006) and the reactions of HO₂·H₂O with HO₂ (Kanno et al., 2006) and NO (Butkovskaya et al., 2007). Finally, in section S1.4, we considered formation of ethyl nitrite and ethyl peroxy nitrate, which are not part of the MCM.

S1.1 MCM only simulations

The chemistry in the PERCA reactor was modelled at temperatures of 25 °C or 250 °C using a subset of the MCM V3.3.1 obtained from <http://mcm.leeds.ac.uk/MCM> by adding ethane to the marked list and extracting the subset in the Kinetic Preprocessor (KPP) (Sandu and Sander, 2006) format along with inorganic reactions and generic rate coefficients. A plug flow modelling approach was used where initial conditions and mixing ratios were set and the model allowed to proceed without any additional inputs or outputs. Radical wall-loss reactions were not added.

Simulations were performed using the optimized PERCA reagent gas concentrations (i.e., 650 ppbv NO; 1.65 % ethane) at either 25 °C or 250 °C. Table S1 provides an overview of the model inputs. The model runs were also initialized with an initial input of 15, 100, 300, 600, 900, or 1200 pptv of either HO₂ or CH₃O₂.

Table S1. Model inputs for simulations run at 25 °C and 250 °C

	Mixing Ratio	Number density at 25 °C (molecules cm ⁻³)	Number density at 250 °C (molecules cm ⁻³)
M	-	2.14×10^{19}	1.22×10^{19}
NO	650 ppbv	1.39×10^{13}	7.92×10^{12}
C ₂ H ₆	1.65%	3.53×10^{17}	2.01×10^{17}
O ₂	20.1%	4.29×10^{18}	2.45×10^{18}
N ₂	77.6%	1.66×10^{19}	9.46×10^{18}

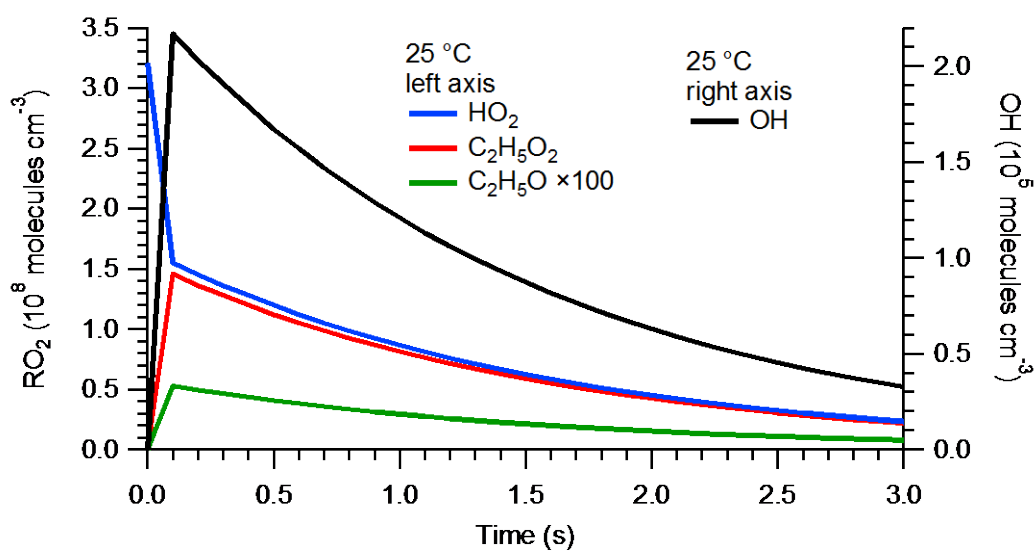


Figure S1. Time series of peroxy radicals (left-hand axis) and hydroxyl radicals (right-hand axis) for a simulation initiated with 15 pptv of HO₂ at 25 °C.

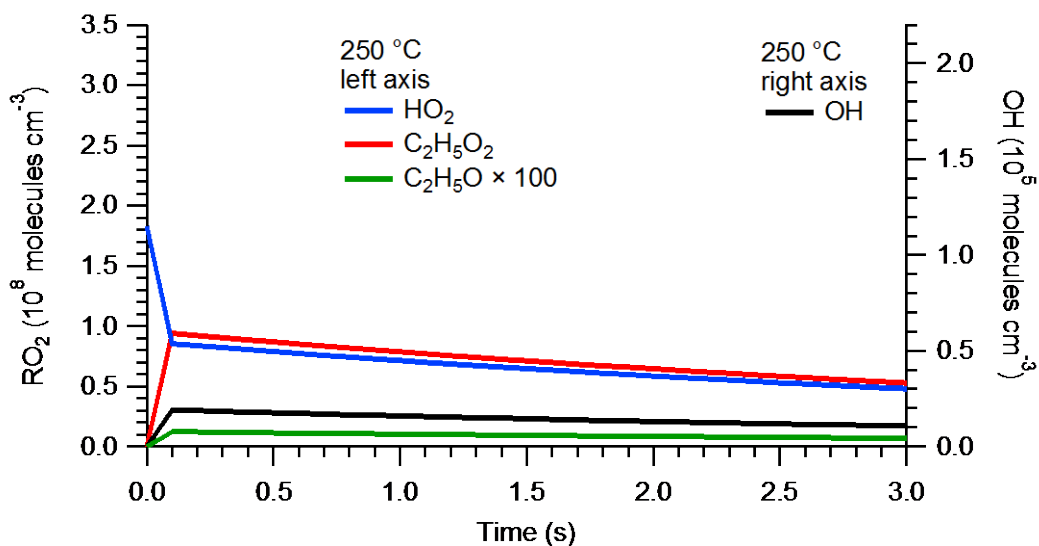


Figure S2. Time series of peroxy radicals (left-hand axis) and hydroxyl radicals for a simulation initiated with 15 pptv of HO₂ at 250 °C.

Figures S1 and S2 show peroxy and hydroxyl radical concentrations during the first 5 seconds of simulations initiated with 15 pptv of HO₂ at 25 °C and 250 °C, respectively. In our chamber, the PERCA reactions are stopped as the radicals encounter the filter after 2.3 s in the dual channel setup. Due to the lower gas density at higher temperatures, a lower concentration of RO₂ radicals is present initially (even though the mixing ratio is the same in both cases). Reactions of HO₂ and RO₂ with NO (e.g., R3, Table 2 of the main manuscript) have negative activation energies and are hence slower at higher temperatures, leading to a lower rate of OH radical production and, since OH loss rates are similar, to lower OH concentrations (maximum of $\sim 1.9 \times 10^4$ molecules cm⁻³ at 250 °C vs. 2.2×10^5 molecules cm⁻³ at 25 °C) and lower turnover numbers.

Figure S3 shows the CL (number of NO₂ molecules produced divided by molecules of RO₂ present originally) as a function of temperature and mixing ratio of radicals added initially. Simulations initiated with HO₂ radicals gave identical results to simulations initiated with CH₃O₂ radicals. For simulations conducted at 25 °C, CL is concentration dependent and decrease with increasing concentration. For simulations conducted at 250 °C, the chain length is still concentration dependent, albeit to a much lesser extent than at room temperature. At 250 °C, the CL in the initial 2.3 s of reaction time is well below the CL obtained at 25 °C, inconsistent with experiment which showed a CL of 69 ± 5 at 250 °C (much higher than CL obtained at 25 °C. This suggests that experimental CL are largely a function of wall reactions not included in the simulations.

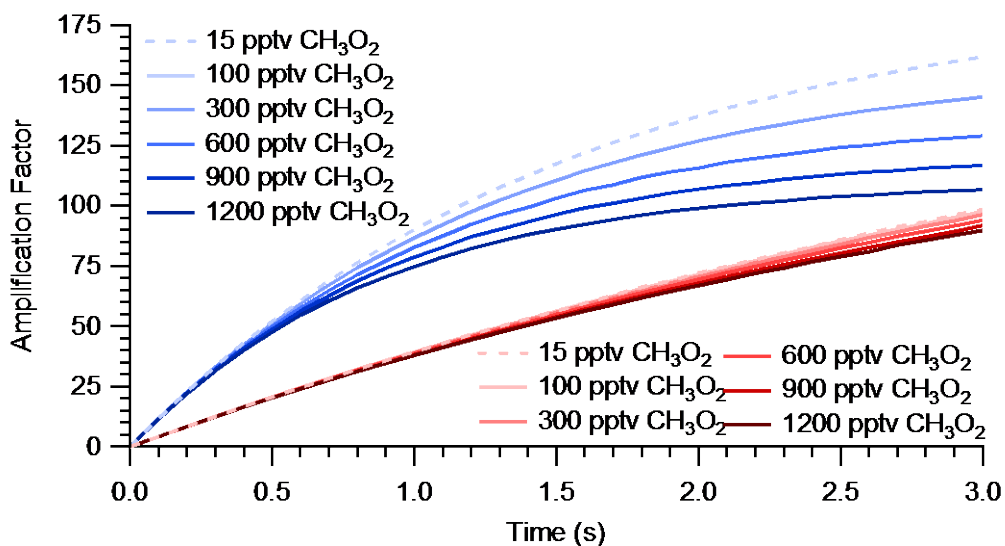


Figure S3. Time series of CL for simulations initiated with 100, 300, 600, 900, and 1200 pptv of CH₃O₂ at 25 °C (blue colors) and 250 °C (red colors).

S1.2 Inclusion of HO₂.H₂O cluster in the mechanism

Another factor contributing to observed CL are radical losses due to HO₂ water cluster formation (i.e., HO₂.H₂O) (Kanno et al., 2006). To estimate the temperature dependent formation of HO₂.H₂O cluster the model assumed that equilibrium between the cluster and HO₂ and H₂O was established at every model time step (0.1 s) following the equilibrium rate constant reported by Kanno et al. (2006): $6.6 \times 10^{-17} \times T \times e^{(3700/T)}$. Upon formation, HO₂.H₂O can react with HO₂ ($k = 6.0 \times 10^{-13} \text{ cm}^3 \text{ molecule}^{-1} \text{ s}^{-1}$) (Kanno et al., 2006) or NO ($k = 5.4 \times 10^{-11} e^{(-410/T)} \text{ cm}^3 \text{ molecule}^{-1} \text{ s}^{-1}$) (Butkovskaya et al., 2007; Butkovskaya et al., 2009).

Figure S4 shows the CL obtained after the inclusion of HO₂.H₂O cluster as a function of RH at 25 °C and 250 °C initiated with 15 pptv HO₂. At 25 °C, the CL is strongly dependent on RH, whereas at 250 °C, there is very little RH dependence as the HO₂.H₂O cluster is thermally dissociated.

Figure S5 shows the concentration dependence at a RH of 20% after inclusion of water clusters in the model simulations. Ultimately, lower CL are observed in the 25 °C system while the 250 °C system chemistry, and associated CL, are relatively unchanged. Furthermore, CLs in the initial 2.3 s of reaction time were generally well below CL obtained at the lower temperature. Once again, this is inconsistent with our experiments where elevated temperatures provided for larger CL values.

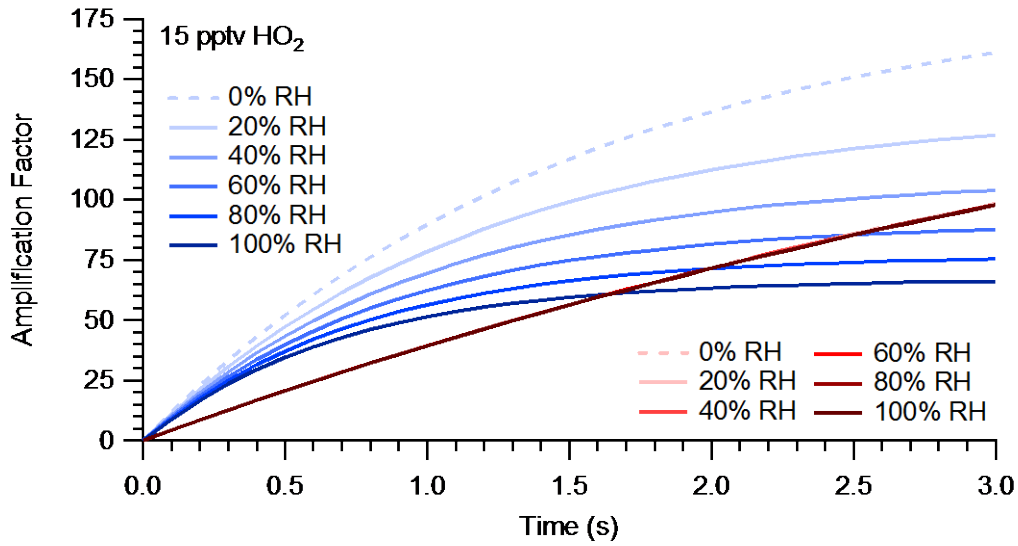


Figure S4. Time series of CL for simulations at different RH and initiated with 15 pptv of HO₂ at 25 °C (blue colors) and 250 °C (red colors).

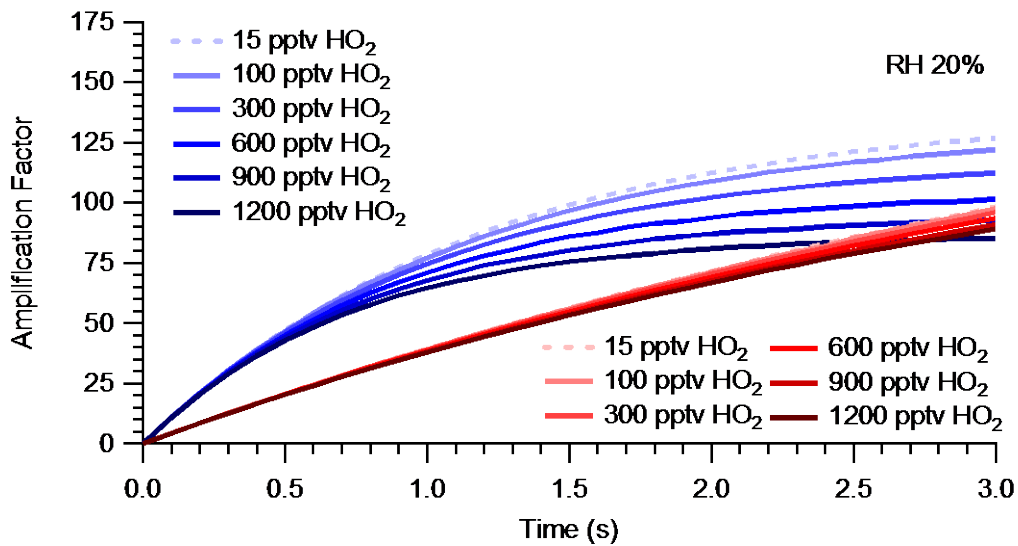


Figure S5. Time series of CL for simulations at 20% RH initiated with different HO₂ mixing ratios at 25 °C (blue colors) and 250 °C (red colors).

S1.3 Inclusion of wall losses in the mechanism

The dependence of CL on temperature and RH in the model simulations shown in S1 and S2 are inconsistent with experiment. To reconcile model simulations with experiment, pseudo-first order wall loss reactions of radicals were added to the mechanism. The room-temperature rate constants reported by Mihele et al. (1999) for HO₂ and RO₂ of 2.8 s⁻¹ and 0.8 s⁻¹ were used, respectively.

Figure S6 shows a time series of the CL for simulations conducted at 20% RH after inclusion of these wall losses in the model. Due to increased radical losses, radical chemistry ceases after ~ 1s. Furthermore, the CL dependence on radical concentration is reduced.

Inconsistent with experiment, the CL is still predicted to be larger at 25 °C than at 250 °C. This may be a result of the use of temperature independent wall loss rates that should be reduced at elevated temperatures.

Assuming, as a lower limit, no wall losses at 250 °C, and factoring in the 2.3 second residence time of our PERCA chamber, the simulations predict larger CL at elevated temperatures (a CL of 80 at 250 °C and a CL of 44 at 25 °C – shown as a green trace in Fig. S6).

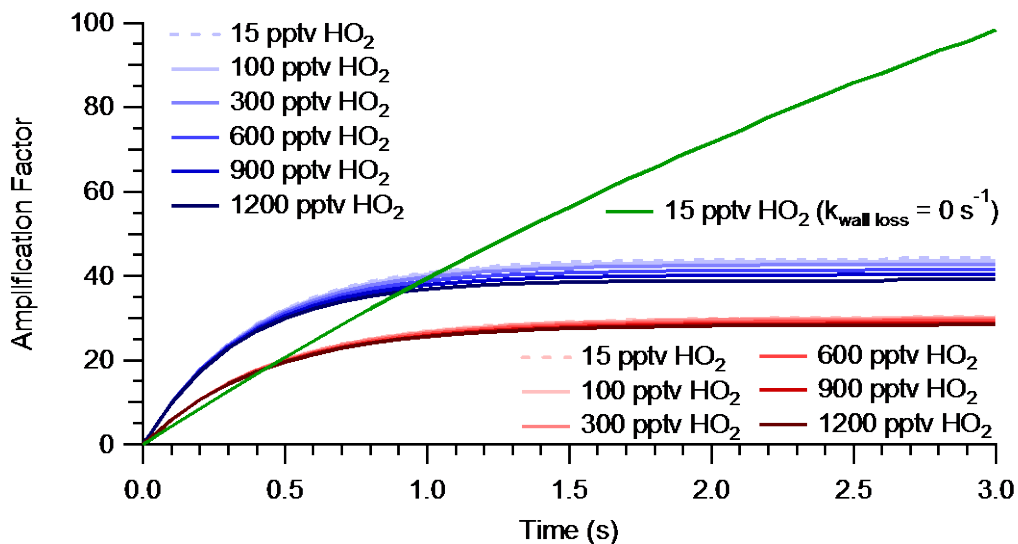


Figure S6. Time series of CL for simulations at 20% RH initiated as a function of HO₂ mixing ratios at 25 °C (blue colors) and 250 °C (red colors) with k_{wall}(HO₂) and k_{wall}(RO₂) of 2.8 s⁻¹ and 0.8 s⁻¹, respectively.

S1.4 Inclusion of ethyl nitrite and ethyl peroxy nitrate formation in the mechanism

A potentially important radical chain termination reaction not included in the MCM is that between $\text{C}_2\text{H}_5\text{O}$ and NO to form $\text{C}_2\text{H}_5\text{ONO}$ (Mihele and Hastie, 2000; Wood et al., 2016). The rate of this reaction decreases slightly with temperature: At a pressure of 660 Torr and using kinetic parameters from (Burkholder et al., 2015), the rate coefficient decreases from 4.8×10^{-11} to $3.9 \times 10^{-11} \text{ cm}^3 \text{ molecule}^{-1} \text{ s}^{-1}$ between 25 °C and 250 °C. Ethyl nitrite thermally decomposes with an activation barrier of $\sim 157 \text{ kJ mol}^{-1}$ (Steacie and Shaw, 1934) and has a lifetime with respect to thermal decomposition (to NO and $\text{C}_2\text{H}_5\text{O}$) of $\sim 40 \text{ s}$ at 250 °C; this implies that for the temperature ranges shown in the manuscript, ethyl nitrite will not significantly decompose and constitutes a radical sink.

Another potentially important radical chain termination reaction not included in the MCM is that between $\text{C}_2\text{H}_5\text{O}_2$ and NO_2 to form $\text{C}_2\text{H}_5\text{O}_2\text{NO}_2$ (Wood et al., 2016). The rate of this reaction also decreases slightly with temperature: at a pressure of 660 Torr and using the kinetic parameters from (Burkholder et al., 2015), the rate coefficient decreases from 8.8×10^{-12} to $8.5 \times 10^{-12} \text{ cm}^3 \text{ molecule}^{-1} \text{ s}^{-1}$ between 25 °C and 250 °C. $\text{C}_2\text{H}_5\text{O}_2\text{NO}_2$ thermally decomposes with an activation barrier of $\sim 86.8 \text{ kJ mol}^{-1}$ and has lifetimes with respect to thermal decomposition (to NO_2 and $\text{C}_2\text{H}_5\text{O}_2$) of $\sim 0.2 \text{ s}$ and $\sim 5 \times 10^{-8} \text{ s}$ at 25 °C and 250 °C, respectively. Formation of this molecule is hence expected to shift radical chemistry at 25 °C while having little effect at 250 °C.

Shown in Figure S7 are the simulations of Figure S6 with $\text{C}_2\text{H}_5\text{ONO}$ and $\text{C}_2\text{H}_5\text{O}_2\text{NO}_2$ formation and thermal decomposition added to the mechanism.

Assuming, as a lower limit, no wall losses at 250 °C, and factoring in the 2.3 s residence time of our PERCA chamber, the simulations predict larger CL at elevated temperatures (a CL of 65 at 250 °C and a CL of 30 at 25 °C – shown as a green trace in Fig. S6). These values are consistent with experiment.

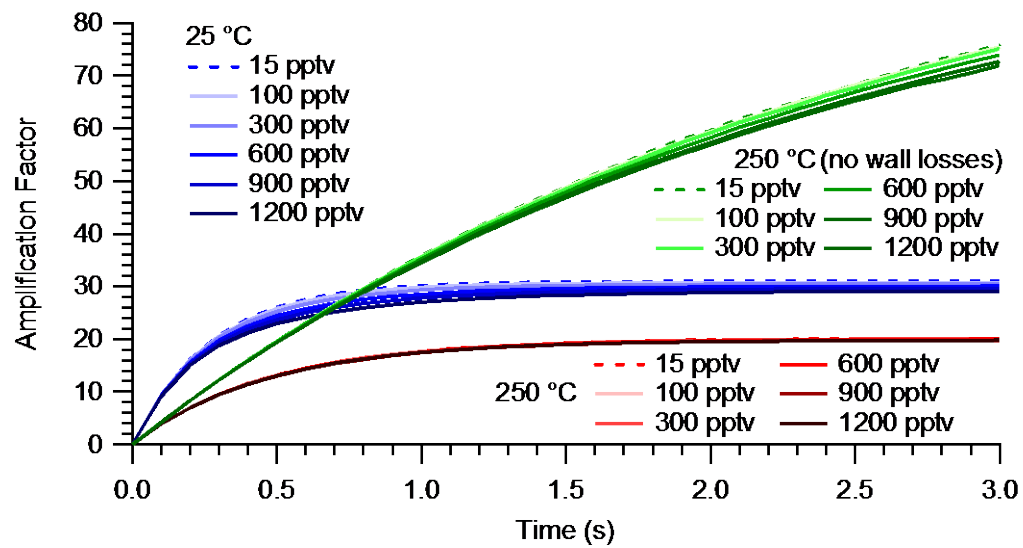


Figure S7. Same as Figure S6 but with C_2H_5ONO and $C_2H_5O_2NO_2$ formation and thermal decomposition included in the mechanism.

References

Burkholder, J. B., Sander, S. P., Abbatt, J. P. D., Barker, J. R., Huie, R. E., Kolb, C. E., Kurylo, M. J., Orkin, V. L., Wilmouth, D. M., and Wine, P. H.: Chemical Kinetics and Photochemical Data for Use in Atmospheric Studies, Evaluation Number 18, National Aeronautics and Space Administration, Jet Propulsion Laboratory, California Institute of Technology, Pasadena, California, 2015.

Butkovskaya, N., Kukui, A., and Le Bras, G.: HNO_3 forming channel of the $\text{HO}_2 + \text{NO}$ reaction as a function of pressure and temperature in the ranges of 72-600 Torr and 223-323 K, *J. Phys. Chem. A*, 111, 9047-9053, 10.1021/jp074117m, 2007.

Butkovskaya, N., Rayez, M. T., Rayez, J. C., Kukui, A., and Le Bras, G.: Water Vapor Effect on the HNO_3 Yield in the $\text{HO}_2 + \text{NO}$ Reaction: Experimental and Theoretical Evidence, *J. Phys. Chem. A*, 113, 11327-11342, 10.1021/jp811428p, 2009.

Jenkin, M. E., Saunders, S. M., and Pilling, M. J.: The tropospheric degradation of volatile organic compounds: a protocol for mechanism development, *Atmos. Environ.*, 31, 81-104, 10.1016/S1352-2310(96)00105-7, 1997.

Jenkin, M. E., Wyche, K. P., Evans, C. J., Carr, T., Monks, P. S., Alfarra, M. R., Barley, M. H., McFiggans, G. B., Young, J. C., and Rickard, A. R.: Development and chamber evaluation of the MCM v3.2 degradation scheme for β -caryophyllene, *Atmos. Chem. Phys.*, 12, 5275-5308, 10.5194/acp-12-5275-2012, 2012.

Kanno, N., Tonokura, K., and Koshi, M.: Equilibrium constant of the $\text{HO}_2\text{-H}_2\text{O}$ complex formation and kinetics of $\text{HO}_2 + \text{HO}_2\text{-H}_2\text{O}$: Implications for tropospheric chemistry, *J. Geophys. Res.-Atmos.*, 111, D20312, 10.1029/2005jd006805, 2006.

Mihele, C. M., Mozurkewich, M., and Hastie, D. R.: Radical loss in a chain reaction of CO and NO in the presence of water: Implications for the radical amplifier and atmospheric chemistry, *Internat. J. Chem. Kin.*, 31, 145-152, 10.1002/(sici)1097-4601(1999)31:2<145::aid-kin7>3.0.co;2-m, 1999.

Mihele, C. M., and Hastie, D. R.: Optimized operation and calibration procedures for radical amplifier-type detectors, *Journal Of Atmospheric And Oceanic Technology*, 17, 788-794, 10.1175/1520-0426(2000)017<0788:OOACPF>2.0.CO;2, 2000.

Sandu, A., and Sander, R.: Technical note: Simulating chemical systems in Fortran90 and Matlab with the Kinetic PreProcessor KPP-2.1, *Atmos. Chem. Phys.*, 6, 187-195, 10.5194/acp-6-187-2006, 2006.

Saunders, S. M., Jenkin, M. E., Derwent, R. G., and Pilling, M. J.: Protocol for the development of the Master Chemical Mechanism, MCM v3 (Part A): tropospheric degradation of non-aromatic volatile organic compounds, *Atmos. Chem. Phys.*, 3, 161-180, 10.5194/acp-3-161-2003, 2003.

Steacie, E. W. R., and Shaw, G. T.: The Homogeneous Unimolecular Decomposition of Gaseous Alkyl Nitrites. II. The Decomposition of Ethyl Nitrite, *The Journal of Chemical Physics*, 2, 345-348, 10.1063/1.1749485, 1934.

Wood, E. C., Deming, B. L., and Kundu, S.: Ethane-Based Chemical Amplification Measurement Technique for Atmospheric Peroxy Radicals, *Environmental Science & Technology Letters*, 4, 15-19, 10.1021/acs.estlett.6b00438, 2016.